OPEN ACCESS Freely available online

PLOS ONE

HHEX Promotes Hepatic-Lineage Specification through the Negative Regulation of Eomesodermin

Hitoshi Watanabe[1☯], Kazuo Takayama[1,2,3☯], Mitsuru Inamura[1], Masashi Tachibana[1], Natsumi Mimura[2], Kazufumi Katayama[1], Katsuhisa Tashiro[4], Yasuhito Nagamoto[1,2], Fuminori Sakurai[1], Kenji Kawabata[4], Miho Kusuda Furue[5,6], Hiroyuki Mizuguchi[1,2,3,7]*

1 Laboratory of Biochemistry and Molecular Biology, Graduate School of Pharmaceutical Sciences, Osaka University, Osaka, Japan, **2** Laboratory of Hepatocyte Differentiation, National Institute of Biomedical Innovation, Osaka, Japan, **3** iPS Cell-Based Research Project on Hepatic Toxicity and Metabolism, Graduate School of Pharmaceutical Sciences, Osaka University, Osaka, Japan, **4** Laboratory of Stem Cell Regulation, National Institute of Biomedical Innovation, Osaka, Japan, **5** Laboratory of Embryonic Stem Cell Cultures, Department of Disease Bioresources Research, National Institute of Biomedical Innovation, Osaka, Japan, **6** Department of Embryonic Stem Cell Research, Field of Stem Cell Research, Institute for Frontier Medical Sciences, Kyoto University, Kyoto, Japan, **7** The Center for Advanced Medical Engineering and Informatics, Osaka University, Osaka, Japan

Abstract

Human embryonic stem cells (hESCs) could provide a major window into human developmental biology, because the differentiation methods from hESCs mimic human embryogenesis. We previously reported that the overexpression of hematopoietically expressed homeobox (HHEX) in the hESC-derived definitive endoderm (DE) cells markedly promotes hepatic specification. However, it remains unclear how HHEX functions in this process. To reveal the molecular mechanisms of hepatic specification by HHEX, we tried to identify the genes directly targeted by HHEX. We found that HHEX knockdown considerably enhanced the expression level of eomesodermin (EOMES). In addition, HHEX bound to the HHEX response element located in the first intron of EOMES. Loss-of-function assays of EOMES showed that the gene expression levels of hepatoblast markers were significantly upregulated, suggesting that EOMES has a negative role in hepatic specification from the DE cells. Furthermore, EOMES exerts its effects downstream of HHEX in hepatic specification from the DE cells. In conclusion, the present results suggest that HHEX promotes hepatic specification by repressing EOMES expression.

Citation: Watanabe H, Takayama K, Inamura M, Tachibana M, Mimura N, et al. (2014) HHEX Promotes Hepatic-Lineage Specification through the Negative Regulation of Eomesodermin. PLoS ONE 9(3): e90791. doi:10.1371/journal.pone.0090791

Editor: Anton Wutz, Wellcome Trust Centre for Stem Cell Research, United Kingdom

Received May 18, 2013; **Accepted** February 5, 2014; **Published** March 20, 2014

Funding: HM and MKF were supported by grants from the Ministry of Health Labor and Welfare of Japan. HM was also supported by The Uehara Memorial Foundation. FS were supported by Program for Promotion of Fundamental Studies in Health Sciences of the National Institute of Biomedical Innovation (NIBIO). K. Takayama and YN are supported by a Grant-in-aid for the Japan Society for the Promotion of Science Fellows. The funders had no role in study design data collection and analysis decision to publish or preparation of the manuscript.

Competing Interests: The authors have declared that no competing interests exist.

* E-mail: mizuguch@phs.osaka-u.ac.jp

☯ These authors contributed equally to this work.

Introduction

The molecular mechanisms of liver development have been clarified by using model organisms such as chicks, *Xenopus*, *zebrafish*, and mice [1–2]. Although these models have many advantages, the molecular mechanisms of human liver development might be different from those of model organisms. The use of differentiation models from human embryonic stem cells (hESCs) for studying human development might resolve these problems, because these differentiation methods mimic human embryogenesis [3]. Previous reports have demonstrated that the definitive endoderm (DE) cells could be efficiently generated from hESCs in the presence of Activin A [4], and that the hESC-derived DE cells have the potential to differentiate into various DE-derived lineages, such as hepatocytes, pancreatic beta-cells, and small intestinal enterocytes[5–7]. In hepatic differentiation, Agarwal et al. reported that the typical gene expression profiles observed in the differentiation model from hESCs are similar to those observed in fetal liver development [8]. In addition, we previously reported that CCAAT/enhancer binding protein-mediated regulation of TGF beta receptor 2 expression determines the hepatoblast fate decision by using a differentiation model from hESCs [9]. The use of differentiation models from hESCs, rather than the usual model organisms, would provide great opportunities to expand our understanding of the molecular mechanisms.

A transcription factor, *hematopoietically expressed homeobox* (HHEX), is initially expressed in DE, and then its expression is restricted to the future hepatoblasts, which could segregate into both hepatocytes and cholangiocytes [10]. In the *HHEX*-null embryo, some hepatic gene expression levels are reduced and further hepatic development is prevented [11–12]. These studies indicate that the transcription factor HHEX plays an essential role in hepatic specification from DE. Recently, we reported that overexpression of HHEX by using adenovirus (Ad) vectors in the hESC-derived DE cells markedly promotes the hepatic specification [13]. Moreover, Kubo et al. demonstrated that HHEX promotes this process by synergistically working with bone morphogenetic protein 4 (BMP4), and they expected that HHEX might function with *HNF1 homeobox A* (HNF1α) [14], which is known to be its co-activator [15]. However, the functions of HHEX in this process

are not well understood, and the target genes of HHEX have not been investigated in detail. Therefore, we attempted to identify the target genes of HHEX in the hepatic specification by using a differentiation model from hESCs.

In the present study, to elucidate the functions of HHEX in hepatic specification from DE, we attempted to identify the target genes of HHEX by using the hepatic differentiation model from hESCs. To this end, the candidate target gene of HHEX were verified by performing ChIP-qPCR and luciferase reporter assays, and then loss-of-function assays were performed to clarify the functions of the candidate target gene in the hepatic specification. These results confirmed that *eomesodermin* (EOMES), which is known to regulate DE differentiation, is one of the crucial target genes of HHEX in human hepatic specification from the DE. Our report thus shows for the first time that HHEX promotes hepatic specification through the repression of EOMES expression.

Materials and Methods

hESCs Culture

A hESC line, H9 (WA09, WISC Bank, WiCell Research Institute), was maintained on a feeder layer of mitomycin C-treated mouse embryonic fibroblasts (MEF) (Millipore) with ReproStem medium (ReproCELL) supplemented with 5 ng/ml fibroblast growth factor 2 (FGF2) (KATAYAMA CHEMICAL INDUSTRIES). hESCs were dissociated with 0.1 mg/ml dispase (Roche) into small clumps and then were subcultured every 4 or 5 days. H9 was used following the Guidelines for Utilization of Human Embryonic Stem Cells of the Ministry of Education, Culture, Sports, Science and Technology of Japan after approval by the institutional ethical review board at National Institute of Biomedical Innovation.

In vitro Differentiation

The differentiation protocol for the induction of DE cells and hepatoblasts was based on our previous report with some modifications [13–16–21]. Briefly, hESCs were dissociated by using dispase and suspended in MEF-conditioned ReproStem medium supplemented with 10 ng/ml FGF2, and then plated onto a growth factor reduced Matrigel (BD Biosciences)-coated dish. When hESCs reached approximately 80% confluence, the MEF-conditioned ReproStem medium was replaced with the differentiation RPMI-1640 medium (Sigma) containing 100 ng/ml Activin A (R&D systems) (the differentiation RPMI-1640 medium is consisted with RPMI-1640 medium (Sigma) supplemented with B27 supplement (Invitrogen) and 4 mM L-glutamine), and then cultured for 4 days. For induction of the hepatoblasts, the DE cells were cultured for 5 days in the differentiation RPMI-1640 medium supplemented with 20 ng/ml BMP4 (R&D Systems) and 20 ng/ml FGF4 (R&D Systems).

RNA Isolation and Reverse Transcription-PCR

Total RNA was isolated from hESCs and their derivatives using ISOGENE (Nippon Gene). cDNA was synthesized using 500 ng of total RNA with a SuperScript VILO cDNA Synthesis Kit (Invitrogen). Real-time RT-PCR was performed with SYBR Green PCR Master Mix (Applied Biosystems) using an Applied Biosystems StemOnePlus real-time PCR systems. Relative quantification was performed against a standard curve and the values were normalized against the input determined for the housekeeping gene, glyceraldehyde 3-phosphate dehydrogenase (GAPDH). The primer sequences used in this study are described in **Table S1 in File S2**.

Flow Cytometry

Single-cell suspensions of the hESC derivatives were fixed with 2% paraformaldehyde (PFA) at 4°C for 20 minutes and then incubated with the primary antibody, followed by the secondary antibody. Flow cytometry analysis was performed using a FACS LSR Fortessa flow cytometer (BD Biosciences). All the antibodies are listed in **Table S2 in File S2**.

ChIP-qPCR

ChIP assays were performed by using a Chromatin Immunoprecipitation Assay Kit (Millipore) according to the manufacturer's instructions. The hESC-derived cells (approximately 1.0×10^6 cells) were cross-linked with 1% formaldehyde at room temperature for 10 minutes. The cells were washed once with PBS containing protease inhibitors (1 mM phenylmethylsulfonyl fluoride, 1 mg/ml aprotinin and 1 mg/ml pepstatin A) and then harvested using a cell scraper. The cross-linked cells were centrifuged and resuspended with sodium dodecyl sulfate (SDS) lysis buffer with the protease inhibitors described above, and then incubated on ice for 10 minutes. The cells were sonicated to solubilize and shear cross-linked DNA. The resulting whole cells were centrifuged, and the supernatants were diluted in ChIP Dilution Buffer containing the protease inhibitors described above, then added to Protein A magnetic beads and rotated at 4°C for 30 minutes. Next, the supernatants of these cells were immunoprecipitated with anti-human HHEX antibody (Santa Cruz Biotechnology, sc-15129) or anti-goat IgG antibody at 4°C overnight with rotation. On the following day, the resulting supernatants were added to Protein A magnetic beads and rotated at 4°C for 60 minutes, then washed five times with Low Salt Immune Complex Wash Buffer (one time), High Salt Immune Complex Wash Buffer (one time), LiCl Immune Complex Wash Buffer (one time), and TE Buffer (two times) for 5 minutes per wash with rotation. Bound complexes were added to elution buffer (1% SDS, 0.1 M $NaHCO_3$) at room temperature for 15 minutes with rotation, and then the supernatants were added to 5 M NaCl and were eluted at 65°C for 4 hours. Immunoprecipitated DNA was purified by treatment with 0.5 M EDTA, 1 M Tris-HCl, and 10 mg/ml proteinase K at 45°C for 60 minutes and recovered by phenol/chloroform alcohol extraction and ethanol precipitation. Purified DNA was used as a template for qPCR according to the protocol described in the *RNA isolation and reverse transcription-PCR* section above. All the antibodies are listed in **Table S2 in File S2**. The primer sequences used in this study are described in **Table S1 in File S2**.

Plasmid Constructions

The promoter region of EOMES was cloned. To generate the 5′ untranslated region (UTR) of the EOMES-firefly luciferase reporter construct (pGL3-EOM-5UTR1000), a 1,000 bp 5′ UTR of the human EOMES was amplified by using the following primers: 5′-AGCGGTACCTTCCTCTCTACAAACCTTTCCCACTGGG-3′ and 5′-TAACCATGGGCTTTGCAAAGCGCAGACGGCAGCTGGCTGC-3′ (−1,000/−1 5′ UTR of EOMES; KpnI and NcoI restriction sites incorporated into sense and antisense primers, respectively, are underlined) and to generate the long 5′ UTR of the EOMES-firefly luciferase reporter construct (pGL3-EOM-5UTR4000), a 4,000 bp 5′ UTR of the human EOMES was amplified by using the following primers: 5′-CAGGGTACCGATAACACGTTTTTAGTGGGGGTG-3′ and 5′-TAACCATGGGCTTTGCAAAGCGCAGACGGCAGCTGGCTGC-3′ (−4,000/−1−5′ UTR of EOMES; KpnI and NcoI restriction sites incorporated into sense and antisense primers, respectively, are underlined).

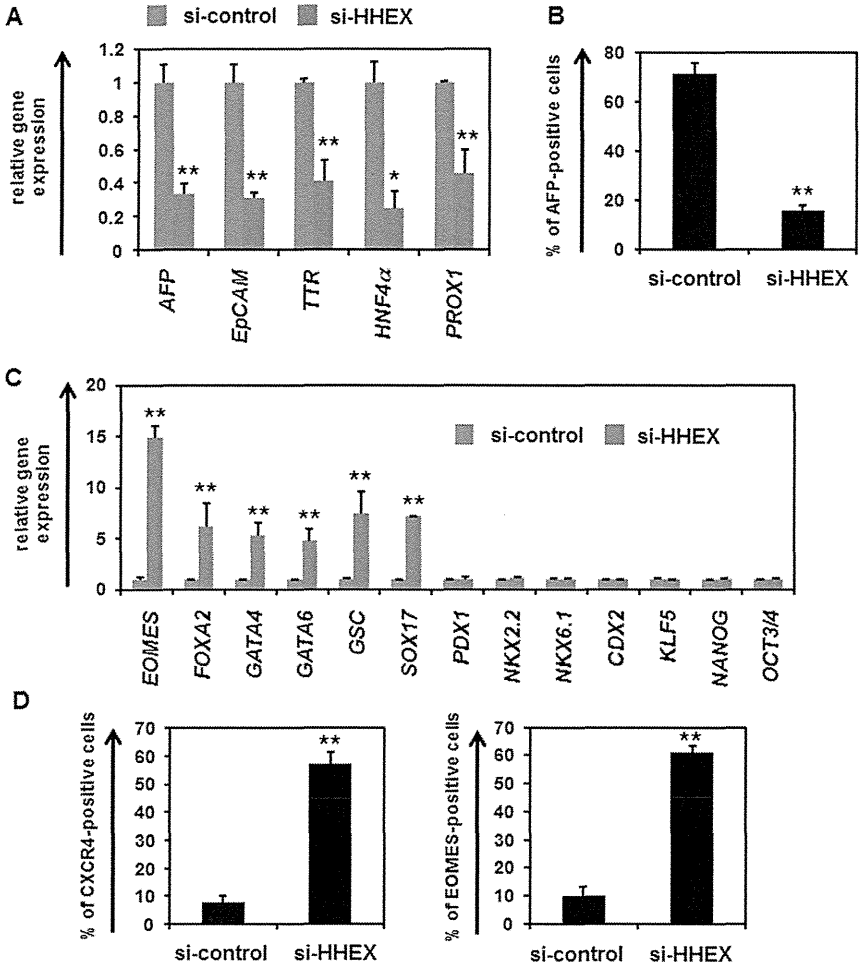

Figure 1. The expression levels of DE markers in the si-HHEX-transfected cells were upregulated in hepatoblast differentiation from DE cells. (**A**) hESCs (H9) were differentiated into DE cells according to the protocol described in the *Materials and Methods* section. The DE cells were transfected with 50 nM si-control or si-HHEX on day 4, and cultured in the medium containing 20 ng/ml BMP4 and 20 ng/ml FGF4 until day 9. On day 9, the gene expression levels of hepatoblast markers (*AFP*, *EpCAM*, *TTR*, *HNF4α*, and *PROX1*) in si-control- or si-HHEX-transfected cells were examined by real-time RT-PCR. The gene expression levels in the si-control-transfected cells were taken as 1.0. (**B**) On day 9, the percentage of AFP-positive cells was measured by using FACS analysis to examine the hepatoblast differentiation efficiency. (**C**) The gene expression levels of DE (*EOMES*, *FOXA2*, *GATA4*, *GATA6*, *GSC*, and *SOX17*), pancreatic (*PDX1*, *NKX2.2*, and *NKX6.1*), intestinal (*CDX2* and *KLF5*), and pluripotent markers (*NANOG* and *OCT3/4*) in the si-control- or si-HHEX-transfected cells were examined by real-time RT-PCR. The gene expression levels in the si-control-transfected cells were taken as 1.0. (**D**) On day 9, the percentage of cells positive for the DE markers (CXCR4 and EOMES) was examined by using FACS analysis. All data are represented as means ± SD ($n = 3$). *$p<0.05$, **$p<0.01$.
doi:10.1371/journal.pone.0090791.g001

Each 5′ UTR of the human EOMES was cloned into the promoter region of the pGL3-Basic vector (Promega) using KpnI and NcoI restriction sites. In addition, the 400 bp region around the HHEX response element (HRE) was amplified by using the following primers: 5′-CCTGCTAGCGTTCTCTGG-TACTTTTCAAAATGGTGC-3′ and 5′-GAAAACTAG-TATGCGCCTGTGCAAGGGAATAGAATCAG-3′. The 400 bp region around the HRE was cloned into the enhancer region of each of pGL3-EOM-5UTR1000 and pGL3-EOM-5UTR4000 using XbaI restriction site to generate pGL3-EOM-5UTR1000 containing the region around the HRE (p5′ EOM-Luc) and pGL3-EOM-5UTR4000 containing the region around the HRE (pLong-5′ EOM-Luc).

To generate pGL3-EOM-5UTR1000 containing the region which has a mutated HRE reporter construct (p5′ EOM-mut-Luc), the following base substitutions were introduced into the 400 bp region around the HRE: 5′-TCCCAATTAAAATC-3′ to 5′-TCC***AGC***T***G***A***C***AATC-3′. PCR products were cloned into the enhancer region of pGL3-EOM-5UTR1000 using XbaI restriction site.

Luciferase Reporter Assays

HeLa cells were transfected with each of the firefly luciferase reporter plasmids described above (p5′ EOM-Luc or p5′ EOM-mut-Luc) or control plasmids, pGL3-Basic vector plasmids (pControl-Luc), by using Lipofectamine 2000 (Invitrogen)-mediated gene transfection according to the manufacturer's instructions. HeLa cells were seeded at a density of 2.0×10^5 cells/well in 24-well tissue culture plates, and cultured for 24 hours before transfection. HeLa cells were transfected with 333 ng/well of each firefly luciferase reporter plasmids (pControl-Luc, p5′ EOM-Luc, or p5′ EOM-mut-Luc), 333 ng/well of HHEX expression plasmids (pHMEF5-HHEX [13]) or blank expression plasmids (pHMEF5), and 333 ng/well of internal control plasmids (pCMV-

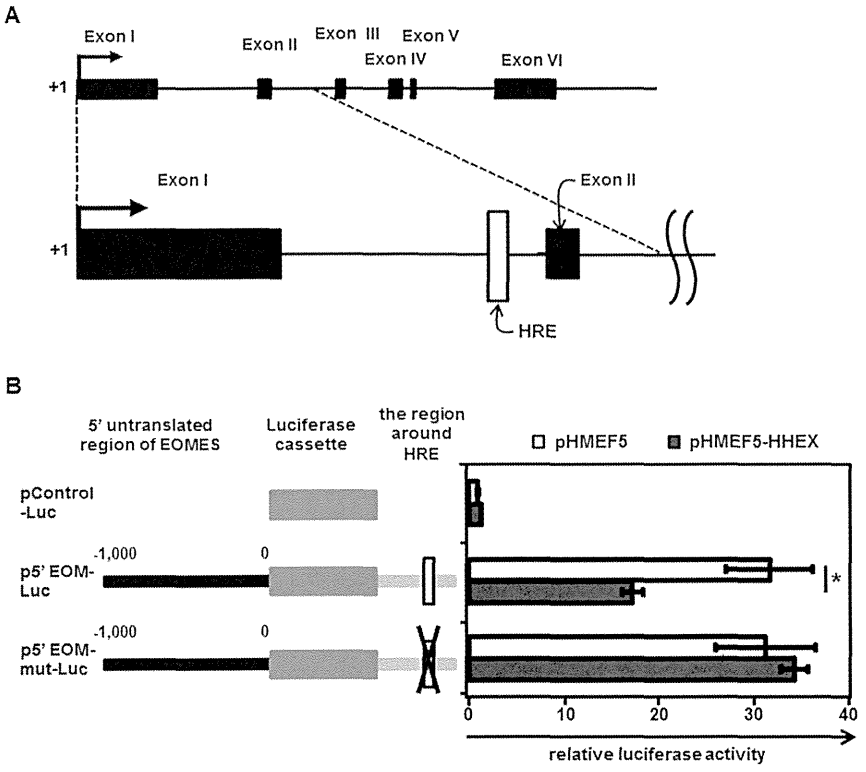

Figure 2. HHEX suppresses EOMES expression by binding to the HRE located in the first intron of EOMES. (**A**) An overview of the EOMES mRNA precursor and the location of the putative HRE are presented. The HRE is located in the first intron of EOMES. (**B**) Luciferase reporter assays were performed to examine the regulation of EOMES expression by HHEX. HeLa cells were cotransfected with both firefly luciferase reporter plasmids (pControl-Luc, p5′ EOM-Luc, or p5′ EOM-mut-Luc) and effecter plasmids (control plasmids (pHMEF5) or HHEX expression plasmids (pHMEF5-HHEX)). The details of the luciferase reporter assays are described in the *Materials and Methods* section. The luciferase activities in the pControl-Luc- and pHMEF5-cotransfected cells were taken as 1.0. All data are represented as means ± SD ($n=3$). *, $p<0.05$.
doi:10.1371/journal.pone.0090791.g002

Renilla luciferase), and cultured for 72 hours. The luciferase activities in the cells were measured by using Dual Luciferase Assay System (Promega) according to the manufacturer's instructions. Firefly luciferase activities in the cells were normalized by the measurement of renilla luciferase activities. The luciferase activity in the cells cotrasfected with pControl-Luc and pHMEF5 was assigned a value of 1.0.

siRNA Transfection

Knockdown of HHEX or EOMES was performed using a specific small interfering RNA (siRNA) fourplex set targeted to HHEX or EOMES, respectively (Darmacon SMARTpool) (Thermo Fisher Scientific). Si-Control (Darmacon siGENOME Non-Targeting siRNA Pool) (Thermo Fisher Scientific) was used as a control. Lipofectamine RNAiMAX (Invitrogen)-mediated gene transfection was used for the reverse transfection according to the manufacturer's instructions. The hESC-derived DE cells on day 4 were transfected with 50 nM of siRNA for 6 hours by reverse transfection.

Immunohistochemistry

The hESC-derived cells were fixed with methanol or 4% PFA. After blocking with PBS containing 1% BSA (Sigma), 0.2% Triton X-100 (Sigma), and 10% FBS, the cells were incubated with primary antibody at 4°C overnight, followed by incubation with a secondary antibody that was labeled with Alexa Fluor 488 (Invitrogen) at room temperature for 1 hour. All the antibodies are listed in **Table S2 in File S2**.

Western Blotting Analysis

The hESC-derived cells were homogenized with lysis buffer (20 mM HEPES, 2 mM EDTA, 10% glycerol, 0.1% SDS, 1% sodium deoxycholate, and 1% Triton X-100) containing a protease inhibitor mixture (Sigma). After being frozen and thawed, the homogenates were centrifuged at 15,000 *g* at 4°C for 10 minutes, and the supernatants were collected. The lysates were subjected to SDS-PAGE on 7.5% polyacrylamide gel and were then transferred onto polyvinylidene fluoride membranes (Millipore). After the reaction was blocked with 1% skim milk in TBS containing 0.1% Tween 20 at room temperature for 1 hour, the membranes were incubated with anti-human HHEX, EOMES, or β-actin antibodies at 4°C overnight, followed by reaction with horseradish peroxidaseconjugated anti-rabbit IgG or anti-mouse IgG antibodies at room temperature for 1 hour. The band was visualized by ECL Plus Western blotting detection reagents (GE Healthcare) and the signals were read using an LAS-4000 imaging system (Fuji Film). All the antibodies are listed in **Table S2 in File S2**.

Results

Obstruction of Hepatoblast Differentiation by HHEX Knockdown Results in Upregulation of the Expression Levels of DE Markers

It is known that HHEX plays an important role in hepatoblast differentiation [11–12–14]. We have previously reported that HHEX overexpression promoted hepatoblast differentiation from

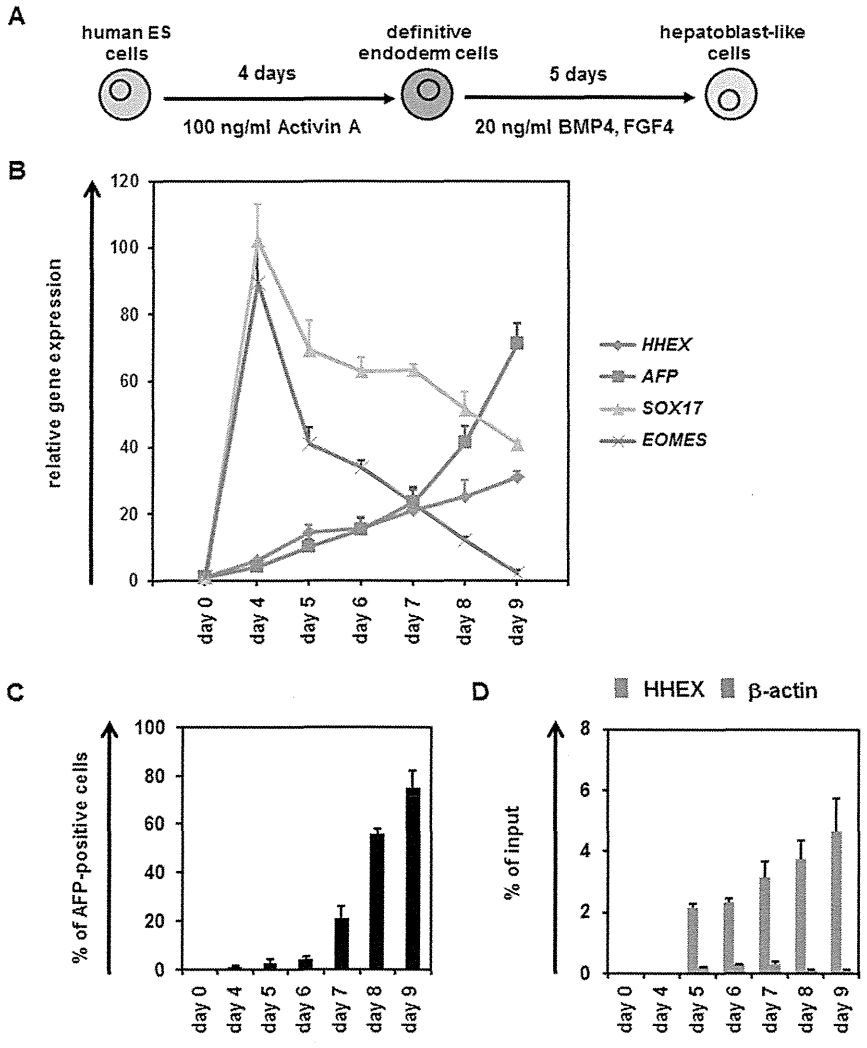

Figure 3. Temporal analysis of endogenous gene expression levels of EOMES and HHEX in hepatoblast differentiation from hESCs. (**A**) The schematic protocol for hepatoblast differentiation from hESCs (H9) is shown. (**B**) The temporal gene expression levels of *HHEX*, *AFP*, *SOX17* and *EOMES* were examined by real-time RT-PCR in hepatoblast differentiation. The gene expression levels in undifferentiated hESCs were taken as 1.0. (**C**) To examine the hepatoblast differentiation efficiency, the percentage of AFP-positive cells was measured by FACS analysis. (**D**) The HHEX protein-binding frequencies of the regions around the HRE of the EOMES gene and a negative control gene (β-ACTIN) were measured by ChIP-qPCR analysis. The results are presented as the percent input of anti-HHEX samples compared with those of anti-IgG samples. All data are represented as means ± SD ($n = 3$).

doi:10.1371/journal.pone.0090791.g003

the hESC-derived DE cells [13]. To confirm the importance of HHEX in hepatoblast differentiation, a loss of function assay of HHEX was performed by using siRNA-mediated HHEX knockdown. We confirmed the knockdown of HHEX expression in the hESC-derived DE cells that has been transfected with si-HHEX (**Fig. S1 in File S1**). The gene expression levels of hepatoblast markers in the si-HHEX-transfected cells were significantly downregulated as compared with those in the si-control-transfected cells (**Fig. 1A**). In addition, the percentage of alpha-fetoprotein (AFP; a hepatoblast marker)-positive cells was decreased by HHEX knockdown on day 9 (**Fig. 1B**). These results suggest that hepatoblast differentiation is prevented by HHEX knockdown, demonstrating that HHEX plays an important role in hepatoblast differentiation from DE cells. To characterize the si-HHEX-transfected cells on day 9, the gene expression levels of DE, pancreatic, intestinal, and pluripotent markers were examined (**Fig. 1C**). Interestingly, the gene expression levels of DE markers were significantly upregulated by HHEX knockdown, although those of pancreatic, intestinal, and pluripotent markers were not changed by HHEX knockdown. Furthermore, the percentage of DE marker (CXCR4 and EOMES)-positive cells was increased by HHEX knockdown (**Fig. 1D**). In addition, the percentage of AFP-positive cells or *EOMES* expression level was decreased or increased, respectively, by HHEX knockdown not only in the DE cells (day 4) but also in the cells starting to commit to hepatoblast (day 5–7) (**Fig. S2 in File S1**). This suggested that HHEX knockdown inhibits hepatoblast differentiation but does not simply change the number of the DE cells. These results suggest that the inhibition of HHEX expression during hepatoblast differentiation results in an increase of DE cells, but not pancreatic, intestinal, or undifferentiated cells.

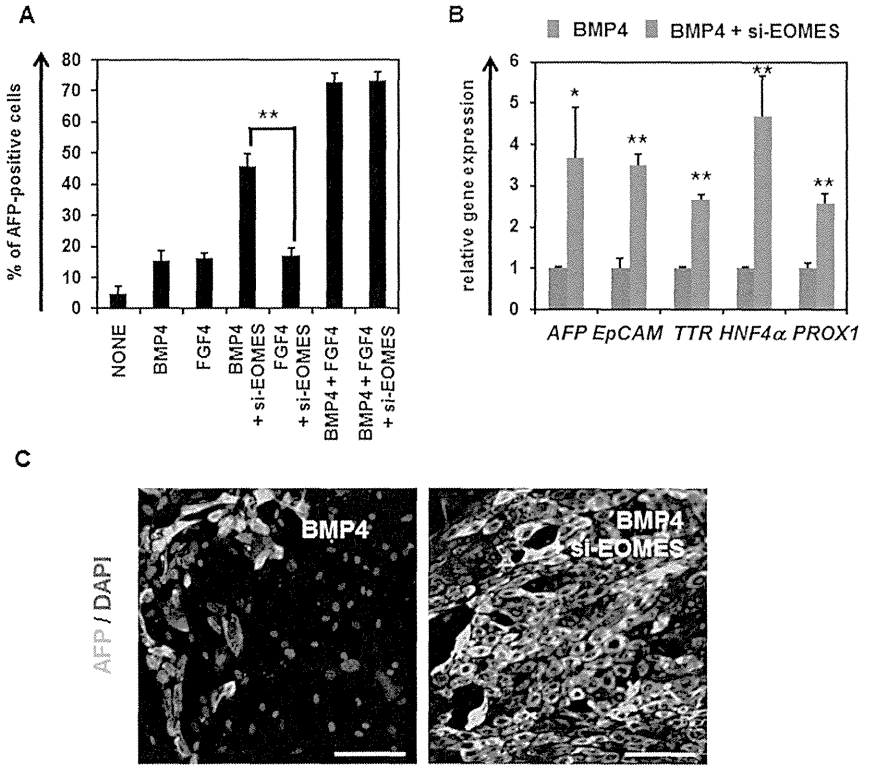

Figure 4. Hepatoblast differentiation was promoted by knockdown of EOMES in the presence of BMP4. (**A**) The hESCs (H9) were differentiated into the DE cells according to the protocol described in the *Materials and Methods* section. The hESC-derived DE cells were transfected with 50 nM si-control or si-EOMES on day 4, and then cultured with the medium containing BMP4 or FGF4. The percentage of AFP-positive cells was examined by FACS analysis on day 9. (**B**) The gene expression levels of hepatoblast markers (*AFP*, *EpCAM*, *TTR*, *HNF4α*, and *PROX1*) were measured by real-time RT-PCR on day 9. The gene expression levels in si-control-transfected cells were taken as 1.0. (**C**) The si-control- or si-EOMES-transfected cells were subjected to immunostaining with anti-AFP (green) antibodies. Nuclei were counterstained with DAPI (blue). The bar represents 50 μm. All data are represented as means ± SD ($n=3$). *$p<0.05$, **$p<0.01$.
doi:10.1371/journal.pone.0090791.g004

HHEX Directly Represses EOMES Expression

Because the gene expression level of *EOMES* was most increased by HHEX knockdown in hepatoblast differentiation, we expected that EOMES might be directly regulated by HHEX. The putative HHEX-binding site (HHEX response element (HRE)) [22] was found in the first intron of EOMES as shown in **Figure 2A**. To investigate whether HHEX could directly repress EOMES transcription, luciferase reporter assays were performed. The reporter plasmids that contain a 5′ untranslated region (UTR) of EOMES (**Fig. S3 in File S1**) and the first intron of EOMES were generated because the putative HHEX-binding site was observed in the first intron of EOMES. The luciferase reporter assays showed that p5' EOM-Luc, which contains the wild-type HRE, mediates significant repression of luciferase activity by HHEX overexpression, whereas p5' EOM-mut-Luc, which contains a mutant HRE, mediates similar luciferase activity even in the presence of HHEX (**Fig. 2B**). These results indicated that HHEX represses EOMES expression through the HRE located in the first intron of EOMES.

Endogenous Temporal Gene Expression Analysis of HHEX and EOMES in Hepatic Specification

To examine the relationship between HHEX and EOMES in hepatic specification, the temporal gene expression patterns of *HHEX* and *EOMES* were examined in hepatoblast differentiation from hESCs (**Fig. 3A**). In DE differentiation (from day 0 to 4), the gene expression levels of *EOMES* and *SOX17* were increased, although those of *HHEX* and *AFP* did not change (**Fig. 3B**). In the hepatic specification process (from day 5 to 9), the gene expression levels of *HHEX* and *AFP* began to be upregulated on day 5, and continued to increase until day 9. On the other hand, the gene expression levels of *EOMES* and *SOX17* started to decrease on day 5, and continued to decrease until day 9. We confirmed that the percentage of CXCR4-positive cells was 95.2±2.2% on day4. In addition, we confirmed that few AFP-positive cells were observed on day 5, and that the percentage of AFP-positive cells continuously increased until day 9 (**Fig. 3C**). To examine whether HHEX binds to the HRE located in the first intron of EOMES, ChIP-qPCR analysis of hepatoblast differentiation from hESCs was performed (**Fig. 3D**). HHEX bound to the HRE located in the first intron of EOMES on day 5, when the hepatic specification began. The amount of HHEX binding to that site continued to increase until day 9. These results suggest that HHEX binds to HRE located in the first intron of EOMES in hepatic specification from the DE cells.

EOMES Knockdown Promotes Hepatic Specification in the Presence of BMP4

To examine the function of EOMES in hepatoblast differentiation, EOMES was knocked down in the DE cells in the presence of BMP4 or FGF4. We confirmed the knockdown of EOMES expression in the hESC-derived DE cells that has been transfected with si-EOMES (**Fig. S4 in File S1**). Although the percentage of AFP-positive cells was increased by EOMES knockdown in the

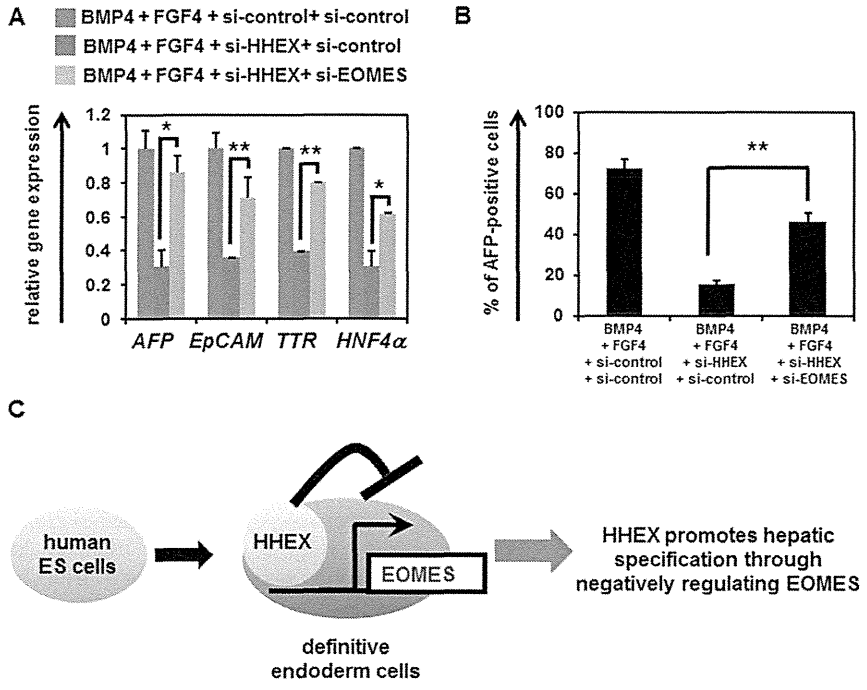

Figure 5. Hepatoblast differentiation is inhibited by EOMES, which functions downstream of HHEX. (**A**) The hESCs (H9) were differentiated into the DE cells according to the protocol described in the *Materials and Methods* section. The hESC-derived DE cells were transfected with 50 nM si-control, si-EOMES, or si-HHEX on day 4, and then cultured with the medium containing BMP4 and FGF4. The gene expression levels of hepatoblast markers (*AFP*, *EpCAM*, *TTR*, and *HNF4α*) were measured by real-time RT-PCR on day 9. The gene expression levels in si-control- and si-HHEX-transfected cells were taken as 1.0. (**B**) The percentage of AFP-positive cells was examined by FACS analysis on day 9. All data are represented as means ± SD ($n = 3$). *$p<0.05$, **$p<0.01$. (**C**) HHEX promotes the hepatic specification from the hESC-derived DE cells by negatively regulating EOMES expression. A model of the hepatic specification from the hESC-derived DE cells by HHEX is presented. In the hESC-derived DE cells, HHEX represses EOMES expression. In this way, HHEX promotes the hepatic specification from the hESC-derived DE cells.
doi:10.1371/journal.pone.0090791.g005

presence of BMP4, it was not changed by EOMES knockdown in the presence of FGF4 (**Fig. 4A**). In addition, EOMES knockdown did not affect the percentage of AFP-positive cells in the presence of both FGF4 and BMP4. This might have been because the endogenous *EOMES* expression level was already sufficiently suppressed under the existence of FGF4 (**Fig. S5 in File S1**). To further investigate the function of EOMES in hepatoblast differentiation, gene expression and immunohistochemical analyses of hepatoblast markers were performed in si-EOMES-transfected cells. The gene expression levels of hepatoblast markers in si-EOMES-transfected cells were upregulated as compared with those in si-control-transfected cells (**Fig. 4B**). Consistently, the immunohistochemical analysis of AFP showed that EOMES knockdown upregulated the expression levels of AFP (**Fig. 4C**). In addition, EOMES knockdown increased the percentage of AFP-positive cells not only in the DE cells (day 4) but also in the cells starting to commit to hepatoblast (day 5–7) (**Fig. S6 in File S1**). This suggested that EOMES knockdown promotes hepatoblast differentiation but does not simply change the number of the DE cells. These results suggest that hepatic specification from the DE cells is promoted by EOMES knockdown depending on the existence of BMP4.

EOMES Functions Downstream of HHEX in the Hepatic Specification from the DE Cells

To examine whether EOMES functions downstream of HHEX in the hepatic specification from the DE cells, both HHEX and EOMES were knocked down in the DE cells, and then the gene expression profiles of hepatoblast markers were analyzed. The gene expression levels of hepatoblast markers were upregulated in both si-HHEX- and si-EOMES-transfected cells as compared with those in si-HHEX-transfected cells (**Fig. 5A**). Furthermore, the percentage of AFP-positive cells was also increased by double-knockdown of HHEX and EOMES (**Fig. 5B**). These results suggest that EOMES knockdown could promote the hepatic specification from the DE cells by HHEX knockdown. In conclusion, EOMES exerts downstream of HHEX in the hepatic specification from the DE cells.

Discussion

The purpose of this study was to identify and characterize the target genes of HHEX in hepatic specification from DE to elucidate the functions of HHEX in this process. We clearly demonstrated that the expression of EOMES is directly suppressed by HHEX, and that EOMES is one of the crucial target genes of HHEX in the hepatic specification from the hESC-derived DE cells. We also showed that EOMES knockdown in the hESC-derived DE cells could rescue the si-HHEX-mediated inhibition of hepatic specification. Our findings indicate that promotion of the hepatic specification by HHEX in the hESC-derived DE cells would be mainly mediated by the repression of EOMES expression (**Fig. 5C**).

To explore direct target genes of HHEX in the hepatic specification, EOMES knockdown experiments were conducted (**Fig. 1**). The luciferase reporter assays (**Fig. 2B**) and ChIP-qPCR (**Fig. 3C**) indicated that HHEX represses EOMES expression by binding to the first intron of EOMES containing a putative HRE. It might be expected that HHEX recruits co-repressor proteins to

repress EOMES expression because HHEX could negatively regulate the expressions of target genes such as *vascular endothelial growth factor (Vegf)* and *vascular endothelial growth factor receptor-1 (Vegfr-1)* by forming the co-repressor protein complexes [23–25]. Previous studies demonstrated that HHEX has three main domains, a repression domain, a DNA-binding domain, and an activation domain [26], and thus exerts both positive and negative effects on the target gene expressions. Taken together, these findings suggested that HHEX would repress EOMES expression through the function of its repression domain.

The results in **figure 4A** demonstrate that EOMES knockdown promoted hepatic specification in the presence of BMP4, but not FGF4. Because it was previously reported that FGF4 could induce the expression level of HHEX in the DE cells [27], FGF4 treatment in the DE cells would lead to downregulation of EOMES expression via the regulation of HHEX expression. Therefore, HHEX and EOMES might exert in the downstream of FGF4 in the hepatic specification. In addition, both BMP4 and FGF4 are necessary for hepatic specification (**Fig. 4A**). However, the functions of BMP4 in hepatic specification and the synergistic effect of BMP and FGF have not been sufficiently elucidated, and will need to be resolved in future studies.

Simultaneous knockdown of HHEX and EOMES in the hESC-derived DE cells led to rescue of the HHEX-mediated inhibition of the hepatic specification (**Fig. 5**). These results suggested that the majority of functions in the hepatic specification by HHEX may be caused by the repression of EOMES expression. EOMES is known to regulate numerous target genes related to DE differentiation, and thus the repression of EOMES expression might also promote other DE-derived lineage specifications, such as pancreatic specification. HHEX is known to regulate not only hepatic specification but also pancreatic specification [11–28]. Therefore, EOMES might also be a target gene of HHEX in pancreatic specification as well as in hepatic specification. Because the HHEX protein is known to interact with the HNF1α protein and synergistically upregulate the HNF1α target gene expression [15], it would be of interest to examine the relationship between HHEX and HNF1α in the hepatic specification from the hESC-derived DE cells. The proteomic analyses of HHEX protein in the hepatic specification from the hESC-derived DE cells might help to elucidate the functions of HHEX in this process.

Conclusions

In summary, we showed that the homeobox gene HHEX promotes the hepatic-lineage specification from the hESC-derived DE cells through the repression of EOMES expression. Previously, we reported that transduction of SOX17, HNF4α, FOXA2 or HNF1α into the hESC-derived cells could promote efficient hepatic differentiation [16–18]. The direct target genes of these genes might be identified by using the strategy described here. Furthermore, identification of the genes targeted by functional genes in the various lineage differentiation models from hESCs will promote understanding of the intricate transcriptional networks that regulate human development.

Supporting Information

File S1 Contains the following files: **Figure S1. Knockdown of HHEX in the DE cells by si-HHEX transfection. (A, B)** The hESCs (H9) were differentiated into the DE cells (day 4) according to the protocol described in *Materials and Methods* section. The DE cells were transfected with 50 nM si-control or si-HHEX on day 4. On day 6, the HHEX expression levels in si-control- or si-HHEX-transfected cells were examined by real-time RT-PCR (**A**) or Western blotting (**B**). The gene expression levels of *HHEX* in the si-control-transfected cells were taken as 1.0. All data are represented as means ± SD ($n = 3$). ** $p<0.01$. **Figure S2. The percentage of AFP-positive cells or *EOMES* expression level was decreased or increased, respectively, by HHEX knockdown. (A, B)** The hESCs (H9) were differentiated into the DE cells according to the protocol described in the *Materials and Methods* section. The DE cells were transfected with 50 nM si-control or si-HHEX on day 4, 5, 6, or 7, and cultured in medium containing 20 ng/ml BMP4 and 20 ng/ml FGF4 until day 9. On day 9, the percentage of AFP-positive cells was measured by using FACS analysis to examine the hepatoblast differentiation efficiency (**A**). Also on day 9, the gene expression levels of EOMES in si-control- or si-HHEX-transfected cells were examined by real-time RT-PCR (**B**). The gene expression levels in the si-control-transfected cells were taken as 1.0. All data are represented as means ± SD ($n = 3$). **$p<0.01$. **Figure S3. Both 1,000 bp and 4,000 bp 5′ UTR of EOMES have promoter activities.** Luciferase reporter assays were performed to examine whether 1,000 bp and 4,000 bp 5′ UTR of EOMES have promoter activity. HeLa cells were cotransfected with both 500 ng/well of firefly luciferase reporter plasmids (pControl-Luc, p5′ EOM-Luc, or pLong-5′ EOM-Luc), and 500 ng/well of internal control plasmids (pCMV-Renilla luciferase), and cultured for 72 hours. The luciferase activities in the cells were measured by using Dual Luciferase Assay System (Promega) according to the manufacturer's instructions. Firefly luciferase activities in the cells were normalized by the measurement of renilla luciferase activities. The RLU in the pControl-Luc-transfected cells was assigned a value of 1.0. All data are represented as means ± SD ($n = 3$). *, $p<0.05$. **Figure S4. Knockdown of EOMES in the DE cells by si-EOMES transfection. (A, B)** The hESCs (H9) were differentiated into the DE cells (day 4) according to the protocol described in *Materials and Methods* section. The DE cells were transfected with 50 nM si-control or si-EOMES on day 4. On day 6, the EOMES expression levels in si-control- or si-EOMES-transfected cells were examined by real-time RT-PCR (**A**) or Western blotting (**B**). The gene expression levels of *EOMES* in the si-control-transfected cells were taken as 1.0. All data are represented as means ± SD ($n = 3$). ** $p<0.01$. **Figure S5. Hepatoblast differentiation was promoted by knockdown of EOMES.** The hESCs (H9) were differentiated into the DE cells according to the protocol described in the *Materials and Methods* section. The hESC-derived DE cells were transfected with 50 nM si-control or si-EOMES on day 4, 5, 6, or 7, and then cultured in medium containing BMP4 or FGF4. The percentage of AFP-positive cells was examined by FACS analysis on day 9. All data are represented as means ± SD ($n = 3$). **$p<0.01$. **Figure S6. The *EOMES* or *HHEX* expression level was suppressed or increased, respectively, in the presence of FGF4.** The hESCs (H9) were differentiated into the DE cells according to the protocol described in the *Materials and Methods* section. The hESC-derived DE cells were cultured in medium containing BMP4 or FGF4 until day 9. The gene expression levels of *EOMES*, *HHEX*, or *AFP* in the non-treated cells (control) were taken as 1.0. All data are represented as means ± SD ($n = 3$). **$p<$ 0.01 (compared with control).
(PDF)

File S2 Contains the following files: **Table S1.** List of primers used in this study. **Table S2.** List of antibodies used in this study.
(DOC)

Acknowledgments

We thank Yasuko Hagihara, Misae Nishijima, Nobue Hirata, and Reiko Hirabayashi for their excellent technical support.

Author Contributions

Conceived and designed the experiments: HW K. Takayama MI MT K. Katayama K. Kawabata HM. Performed the experiments: HW K. Takayama MI NM. Analyzed the data: HW K. Takayama MI MT K. Katayama K. Tashiro YN FS K. Kawabata MKF HM. Wrote the paper: HW K. Takayama HM. Contributed equally to this work: HW K. Takayama.

References

1. Zaret KS, Grompe M (2008) Generation and regeneration of cells of the liver and pancreas. Science 322: 1490–1494.
2. Si-Tayeb K, Lemaigre FP, Duncan SA (2010) Organogenesis and development of the liver. Dev Cell 18: 175–189.
3. Thomson JA, Itskovitz-Eldor J, Shapiro SS, Waknitz MA, Swiergiel JJ, et al. (1998) Embryonic stem cell lines derived from human blastocysts. Science 282: 1145–1147.
4. D'Amour KA, Agulnick AD, Eliazer S, Kelly OG, Kroon E, et al. (2005) Efficient differentiation of human embryonic stem cells to definitive endoderm. Nat Biotechnol 23: 1534–1541.
5. D'Amour KA, Bang AG, Eliazer S, Kelly OG, Agulnick AD, et al. (2006) Production of pancreatic hormone-expressing endocrine cells from human embryonic stem cells. Nat Biotechnol 24: 1392–1401.
6. Si-Tayeb K, Noto FK, Nagaoka M, Li J, Battle MA, et al. (2010) Highly efficient generation of human hepatocyte-like cells from induced pluripotent stem cells. Hepatology 51: 297–305.
7. Spence JR, Mayhew CN, Rankin SA, Kuhar MF, Vallance JE, et al. (2011) Directed differentiation of human pluripotent stem cells into intestinal tissue in vitro. Nature 470: 105–109.
8. Agarwal S, Holton KL, Lanza R (2008) Efficient differentiation of functional hepatocytes from human embryonic stem cells. Stem Cells 26: 1117–1127.
9. Takayama K, Kawabata K, Nagamoto Y, Inamura M, Ohashi K, et al. (2014) CCAAT/enhancer binding protein-mediated regulation of TGFbeta receptor 2 expression determines the hepatoblast fate decision. Development 141: 91–100.
10. Bogue CW, Ganea GR, Sturm E, Ianucci R, Jacobs HC (2000) Hex expression suggests a role in the development and function of organs derived from foregut endoderm. Dev Dyn 219: 84–89.
11. Bort R, Signore M, Tremblay K, Martinez Barbera JP, Zaret KS (2006) Hex homeobox gene controls the transition of the endoderm to a pseudostratified, cell emergent epithelium for liver bud development. Dev Biol 290: 44–56.
12. Keng VW, Yagi H, Ikawa M, Nagano T, Myint Z, et al. (2000) Homeobox gene Hex is essential for onset of mouse embryonic liver development and differentiation of the monocyte lineage. Biochem Biophys Res Commun 276: 1155–1161.
13. Inamura M, Kawabata K, Takayama K, Tashiro K, Sakurai F, et al. (2011) Efficient Generation of Hepatoblasts From Human ES Cells and iPS Cells by Transient Overexpression of Homeobox Gene HEX. Mol Ther 19: 400–407.
14. Kubo A, Kim YH, Irion S, Kasuda S, Takeuchi M, et al. (2010) The homeobox gene Hex regulates hepatocyte differentiation from embryonic stem cell-derived endoderm. Hepatology 51: 633–641.
15. Tanaka H, Yamamoto T, Ban T, Satoh S, Tanaka T, et al. (2005) Hex stimulates the hepatocyte nuclear factor 1alpha-mediated activation of transcription. Arch Biochem Biophys 442: 117–124.
16. Takayama K, Inamura M, Kawabata K, Tashiro K, Katayama K, et al. (2011) Efficient and Directive Generation of Two Distinct Endoderm Lineages from Human ESCs and iPSCs by Differentiation Stage-Specific SOX17 Transduction. PLoS One 6: e21780.
17. Takayama K, Inamura M, Kawabata K, Katayama K, Higuchi M, et al. (2012) Efficient Generation of Functional Hepatocytes From Human Embryonic Stem Cells and Induced Pluripotent Stem Cells by HNF4alpha Transduction. Mol Ther 20: 127–137.
18. Takayama K, Inamura M, Kawabata K, Sugawara M, Kikuchi K, et al. (2012) Generation of metabolically functioning hepatocytes from human pluripotent stem cells by FOXA2 and HNF1alpha transduction. J Hepatol 57: 628–636.
19. Takayama K, Kawabata K, Nagamoto Y, Kishimoto K, Tashiro K, et al. (2013) 3D spheroid culture of hESC/hiPSC-derived hepatocyte-like cells for drug toxicity testing. Biomaterials 34: 1781–1789.
20. Nagamoto Y, Tashiro K, Takayama K, Ohashi K, Kawabata K, et al. (2012) The promotion of hepatic maturation of human pluripotent stem cells in 3D co-culture using type I collagen and Swiss 3T3 cell sheets. Biomaterials 33: 4526–4534.
21. Takayama K, Nagamoto Y, Mimura N, Tashiro K, Sakurai F, et al. (2013) Long-Term Self-Renewal of Human ES/iPS-Derived Hepatoblast-like Cells on Human Laminin 111-Coated Dishes. Stem Cell Reports 1: 322–335.
22. Cong R, Jiang X, Wilson CM, Hunter MP, Vasavada H, et al. (2006) Hhex is a direct repressor of endothelial cell-specific molecule 1 (ESM-1). Biochem Biophys Res Commun 346: 535–545.
23. Noy P, Williams H, Sawasdichai A, Gaston K, Jayaraman PS (2010) PRH/Hhex controls cell survival through coordinate transcriptional regulation of vascular endothelial growth factor signaling. Mol Cell Biol 30: 2120–2134.
24. Guiral M, Bess K, Goodwin G, Jayaraman PS (2001) PRH represses transcription in hematopoietic cells by at least two independent mechanisms. J Biol Chem 276: 2961–2970.
25. Swingler TE, Bess KL, Yao J, Stifani S, Jayaraman PS (2004) The proline-rich homeodomain protein recruits members of the Groucho/Transducin-like enhancer of split protein family to co-repress transcription in hematopoietic cells. J Biol Chem 279: 34938–34947.
26. Crompton MR, Bartlett TJ, MacGregor AD, Manfioletti G, Buratti E, et al. (1992) Identification of a novel vertebrate homeobox gene expressed in haematopoietic cells. Nucleic Acids Res 20: 5661–5667.
27. Morrison GM, Oikonomopoulou I, Migueles RP, Soneji S, Livigni A, et al. (2008) Anterior definitive endoderm from ESCs reveals a role for FGF signaling. Cell Stem Cell 3: 402–415.
28. Bort R, Martinez-Barbera JP, Beddington RS, Zaret KS (2004) Hex homeobox gene-dependent tissue positioning is required for organogenesis of the ventral pancreas. Development 131: 797–806.

STEM CELLS AND DEVELOPMENT
Volume 23, Number 18, 2014

DOI: 10.1089/scd.2013.0469

Plasma Elevation of Vascular Endothelial Growth Factor Leads to the Reduction of Mouse Hematopoietic and Mesenchymal Stem/Progenitor Cells in the Bone Marrow

Katsuhisa Tashiro,[1,*] Aki Nonaka,[1,2,*] Nobue Hirata,[1] Tomoko Yamaguchi,[1] Hiroyuki Mizuguchi,[3–6] and Kenji Kawabata[1,2]

Vascular endothelial growth factor (VEGF) is reported to exhibit potent hematopoietic stem/progenitor cell (HSPC) mobilization activity. However, the detailed mechanisms of HSPC mobilization by VEGF have not been examined. In this study, we investigated the effect of VEGF on bone marrow (BM) cell and the BM environment by intravenous injection of VEGF-expressing adenovirus vector (Ad-VEGF) into mice. A colony assay using peripheral blood cells revealed that plasma elevation of VEGF leads to the mobilization of HSPCs into the circulation. Granulocyte colony-stimulating factor (G-CSF) is known to mobilize HSPCs by decreasing CXC chemokine ligand 12 (CXCL12) levels in the BM. However, we found almost no changes in the CXCL12 levels in the BM after Ad-VEGF injection, suggesting that VEGF can alter the BM microenvironment by different mechanisms from G-CSF. Furthermore, flow cytometric analysis and colony forming unit-fibroblast assay showed a reduction in the number of mesenchymal progenitor cells (MPCs), which have been reported to serve as niche cells to support HSPCs, in the BM of Ad-VEGF-injected mice. Adhesion of donor cells to the recipient BM after transplantation was also impaired in mice injected with Ad-VEGF, suggesting a decrease in the niche cell number. We also observed a dose-dependent chemoattractive effect of VEGF on primary BM stromal cells in vitro. These data suggest that VEGF alters the distribution of MPCs in the BM and can also mobilize MPCs to peripheral tissues. Taken together, our results imply that VEGF-elicited egress of HSPCs would be mediated, in part, by changing the number of MPCs in the BM.

Introduction

HEMATOPOIETIC STEM CELLS (HSCs) sustain blood production throughout life. In a steady state, HSCs exist within the bone marrow (BM) and remain largely quiescent and self-renew at a low rate to avoid their exhaustion. By contrast, HSCs can actively proliferate, differentiate into progenitor cells, or egress from the BM into the circulation in some situations, such as tissue damage-induced cell death and increased plasma levels of hematopoietic cytokines, including the granulocyte colony-stimulating factor (G-CSF). These dynamic behaviors of HSCs are controlled by a local specific microenvironment called niches [1–8]. The non-hematopoietic cells, such as endosteal osteoblasts and perivascular mesenchymal progenitor cells (MPCs), are reported to function as niche cells by supplying several HSC maintenance factors, including the CXC chemokine ligand 12 (CXCL12). Indeed, previous studies have shown that decreased levels of CXCL12 in the BM caused hematopoietic stem/progenitor cell (HSPC) mobilization, indicating the pivotal role of CXCL12 signaling in HSPC egress [9,10].

Not only is the vascular endothelial growth factor (VEGF) a well-known factor in angiogenesis, but it also plays an important role in the growth and differentiation of hematopoietic cells. Homozygous or heterozygous deletion of VEGF in mice leads to early embryonic lethality because of impaired vascular angiogenesis and hematopoiesis [11,12]. By conditional deletion of VEGF in hematopoietic cells, but not in stromal cells, Ferrara and colleagues clearly showed that VEGF is required for survival and repopulation

[1]Laboratory of Stem Cell Regulation, National Institute of Biomedical Innovation, Osaka, Japan.
Laboratory of [2]Biomedical Innovation and [3]Biochemistry and Molecular Biology, Graduate School of Pharmaceutical Sciences, Osaka University, Osaka, Japan.
[4]iPS Cell-Based Research Project on Hepatic Toxicity and Metabolism, Graduate School of Pharmaceutical Sciences, Osaka University, Osaka, Japan.
[5]Laboratory of Hepatocyte Regulation, National Institute of Biomedical Innovation, Osaka, Japan.
[6]The Center for Advanced Medical Engineering and Informatics, Osaka University, Osaka, Japan.
*These two authors contributed equally to this work.

of adult HSCs [13]. Furthermore, VEGF has been shown to be an essential factor for HSC niche formation through endochondral ossification [14]. These observations clearly demonstrate that VEGF exerts physiological actions on hematopoietic systems through both cell-autonomous and -nonautonomous mechanisms.

In addition to the functions described above, VEGF also has a potent HSPC mobilization capacity [15], although the mechanisms of VEGF-induced HSPC mobilization have not been addressed in detail. In the current study, we investigated the effect of VEGF on the BM cell mobilization and BM environment after the intravenous injection of VEGF-expressing adenovirus (Ad) vector (Ad-VEGF) into mice. The results showed that VEGF overexpression in mice could lead to a reduction of not only the HPSC number, but also the MPC number in the BM. We also observed an enhanced chemoattractive activity of BM stromal cells by VEGF. Our data suggest that the plasma elevation of VEGF in mice alters the distribution of MPCs in the BM, and this might cause HSPC egress from the BM.

Materials and Methods

Ad vectors

Ad vectors were constructed by an improved in vitro ligation method [16,17]. The mouse $VEGF_{165}$ cDNA and human G-CSF cDNA were obtained from pBLAST49-mVEGF and pORF9-hGCSFb, respectively (Invivogen). Each cDNA was cloned into a multicloning site of pHMCMV10 [18,19], which contains the cytomegalovirus (CMV) promoter/enhancer and intron A sequence flanked by the I-*Ceu*I and PI-*Sce*I sites, thereby resulting in pHMCMV10-VEGF and pHMCMV10-G-CSF. pHMCMV10-VEGF and pHMCMV10-G-CSF were digested with I-*Ceu*I/PI-*Sce*I and ligated into I-*Ceu*I/PI-*Sce*I-digested pAdHM41-K7 (C) [20], resulting in pAd-VEGF and pAd-G-CSF, respectively. To generate the virus, Ad vector plasmids were digested with *Pac*I and purified by phenol–chloroform extraction and ethanol precipitation. Linearized DNAs were transfected into 293 cells with SuperFect (Qiagen) according to the manufacturer's instructions. The viruses were amplified in 293 cells. Before virus purification, the cell lysates were centrifuged to remove cell debris and were digested for 30 min at 37°C with 200 μg/mL DNase I and 200 μg/mL RNase A in the presence of 10 mM $MgCl_2$. Viruses were purified by $CsCl_2$ step gradient ultracentrifugation followed by $CsCl_2$ linear gradient ultracentrifugation. The purified viruses were dialyzed against a solution containing 10 mM Tris-HCl (pH 7.5), 1 mM $MgCl_2$, and 10% glycerol and were stored at −80°C. The control vector, Ad-Null, is similar in design, except that it contains no transgene in the expression cassette. The biological titers [infectious unit (ifu)] of Ad-VEGF, Ad-G-CSF, and Ad-Null were determined by using an Adeno-X Rapid Titer kit (Clontech).

Administration of Ad vectors in mice

C57BL/6j female mice aged 7–9 weeks were obtained from Nippon SLC, and all animals were maintained under specific pathogen-free conditions. Each Ad vector was intravenously injected into C57BL/6j mice at 1×10^9 ifu through the tail vein. All experiments were conducted according to the institutional ethics guidelines for animal experimentation of the National Institute of Biomedical Innovation.

Cell preparation

Blood and BM were harvested from mice using standard methods on day 5 after injection of Ad vector into mice, and the number of nucleated cells in these tissues was then counted using a Nucleocounter (Chemometec). To collect the nonhematopoietic cells from the femur and tibia, the bone fragments were minced with scissors, and were then incubated at 37°C with a type I collagenase (3 mg/mL; Worthington) in the Dulbecco's modified Eagle's medium (DMEM) with 10% fetal bovine serum (FBS) for 90 min [21]. The cells were filtered with a cell strainer to remove debris and bone fragments, and suspended in a staining buffer [phosphate buffer saline (PBS)/2% FBS]. These cell suspensions were kept on ice for further analysis.

Flow cytometry

The following antibodies (Abs), conjugated with fluorescein isothiocyanate (FITC), phycoerythrin (PE), allophycocyanin (APC), or PECy7, were used for flow cytometric analysis and cell sorting: biotinylated lineage cocktail [CD3 (145-2C11), B220 (RA3-6B2), Gr-1 (RB6-8C5), CD11b (M1/70), Ter119 (Ter-119)], c-Kit-APC (2B8), Sca-1-PECy7 (D7), Ter119-FITC (Ter-119), CD45-FITC (30-F11), CD11b-FITC (M1/70), Gr-1-PE (RB6-8C5), CD31-FITC (390), CD31-APC (390), CD51-PE (RMV-7), PDGFRa-APC (APA-5), Flt-1-PE (141522), Flk1-PE (Avas12a1), and Alcam-PE. For detection of biotinylated Abs, PerCP-Cy5.5- or FITC-conjugated streptavidin was used. Abs were purchased from e-Bioscience, BD Bioscience, Biolegend, and R&D Systems. Cells were incubated with primary Abs at 4°C for 30 min and washed twice with PBS/2% FBS. After staining, cells were analyzed and isolated by flow cytometry on an LSR II and FACSAria flow cytometer, respectively, using FACSDiva software (BD Bioscience).

Enzyme linked immunosorbent assay

Blood samples were collected through the inferior vena cava on day 5 after Ad vector injection, and transferred to polypropylene tubes containing heparin. Plasma was harvested by centrifugation. The BM supernatant was obtained by flushing a femur with 500 μL of PBS, followed by centrifugation at 500*g* for 5 min. The levels of VEGF and CXCL12 in the plasma and BM supernatant were measured using a commercial ELISA kit (R&D Systems) following the manufacturer's instructions.

Reverse transcription-polymerase chain reaction analysis

CD45-negative($^-$) $Ter119^-$ nonhematopoietic cells in the BM were sorted from mice injected with Ad-VEGF or Ad-Null, and total RNA was then extracted using ISOGEN (Nippon Gene). cDNA was synthesized from DNase I-treated total RNA with a Superscript VILO cDNA synthesis kit

(Invitrogen), and quantitative real-time reverse transcription-polymerase chain reaction was performed using the Fast SYBR Green Master Mix with an ABI StepOne Plus system (Applied Biosystems). Relative quantification was performed against a standard curve and the values were normalized against the input determined for the housekeeping gene, glyceraldehyde 3-phosphate dehydrogenase. The sequences of the primers used in this study are listed in Table 1.

Colony assay

BM cells (2×10^4 cells) and peripheral blood cells (2×10^5 cells) were plated in the Methocult M3434 medium (StemCell Technologies, Inc.). Cultures were plated in duplicate and placed in a humidified chamber with 5% CO_2 at 37°C for 10 days. The number of individual colonies was counted by microscopy. The colony number was normalized to the total number of the nucleated cells.

Colony forming unit-fibroblast assay

BM-derived $CD45^-Ter119^-$ cells were added to the MesenCult MSC Basal Medium, including supplements (Stem Cell Technologies, Inc.), and then plated on a six-well plate at 1×10^5 cells per well. Cells were cultured for 14 days and stromal cell colonies (fibroblast-like colonies: >50 cells) derived from colony forming unit-fibroblasts (CFU-Fs) were stained with the Giemsa solution (Wako) after fixation with methanol. The colony number was counted by microscopy.

Cell migration assay

BM-derived stromal cells, including MPCs, were tested for migration toward VEGF using 8-μm pore-sized cell culture inserts (BD Falcon). Stromal cells (1×10^5 cells) resuspended in 200 μL of DMEM/2% FBS were added to the upper chamber, and 750 μL of DMEM/2% FBS containing recombinant mouse VEGF (10 or 100 ng/mL; Peprotech) was added to the bottom chamber. After 6 h of incubation at 37°C, the upper side of the filters was carefully washed with PBS, and cells remaining on the upper face of the filters were removed with a cotton wool swab. The filters were fixed with 100% methanol and stained with the Giemsa solution. Cells migrating into the lower compartment were counted manually in three random microscopic fields (×200).

Homing assay

Mice were administrated with Ad-Null or Ad-VEGF at 1×10^9 ifu. Five days later, BM cells (1×10^7 cells) derived from green fluorescent protein (GFP)-expressing transgenic mice [22] were intravenously transplanted into Ad-Null- or Ad-VEGF-injected mice. At 16 h after BM transplantation, the percentage of GFP-expressing donor cells in the BM was determined by flow cytometry.

Results

Effect of systemic VEGF overexpression on the distribution of myeloid cells and HSPCs in mice

To evaluate the effect of VEGF on the mobilization of hematopoietic cells, we generated a VEGF-expressing Ad vector, Ad-VEGF, because plasma VEGF levels were rapidly decreased with a $t_{1/2}$ of ~25 min after intravenous injection of recombinant VEGF [23]. Single intravenous injection of Ad-VEGF (1×10^9 ifu) into mice led to a significant elevation of VEGF levels in plasma on day 5 compared with Ad-Null-injected mice (control mice) (Fig. 1a). On the other hand, unexpectedly, BM VEGF levels in the Ad-VEGF-injected mice were almost equivalent to those in the Ad-Null-injected mice (Fig. 1b). There were no signs of toxicity in mice treated with Ad-VEGF and Ad-Null at this dose (1×10^9 ifu). To investigate whether the hematopoietic cells could be mobilized from the BM into the circulation after injection of Ad-VEGF, we examined the number of total nucleated cells, myeloid cells ($Gr\text{-}1^+CD11b^+$ cells), and HSPCs [$c\text{-}Kit^+Sca\text{-}1^+Lineage^-$ (KSL) cells or CFU-granulocyte, erythroid, macrophage, megakaryocyte/CFU-Mix] in the peripheral blood. Compared with Ad-Null-injected mice, Ad-VEGF-injected mice showed an increased number of total nucleated cells and myeloid cells in the peripheral blood (Fig. 1c, d). We found that the number of multipotent hematopoietic progenitor cells, CFU-GEMM/CFU-Mix, in the blood of Ad-VEGF-injected mice was four times as great as that of Ad-Null-injected mice (Fig. 1e). Importantly, in Ad-VEGF-injected mice, the number of KSL cells in the blood was also increased (Fig. 1f). These results indicate that hematopoietic cells, including immature hematopoietic cells with colony-forming potentials, would be mobilized from the BM following systemic Ad-VEGF administration.

An increased number of mobilized cells in VEGF-treated mice were reported previously [15], but little is known about the effect of VEGF on BM cells during the mobilization period. Thus, we next investigated the number of total BM cells, myeloid cells, and HSPCs. In contrast to the peripheral blood, the number of total hematopoietic cells, myeloid cells, and CFU-Mix was significantly decreased (Fig. 2a–c). It is of note that the VEGF overexpression in mice resulted

TABLE 1. PRIMER SEQUENCES USED IN THIS STUDY

Gene name	*(5′) Sense primers (3′)*	*(5′) Antisense primers (3′)*
Gapdh	TTCACCACCATGGAGAAGAAGGC	GGCATGGACTGTGGTCATGA
Cdh2	CAAGAGCTTGTCAGAATCAGG	CATTTGGATCATCCGCATC
Vcam-1	GACCTGTTCCAGCGAGGGTCTA	CTTCCATCCTCATAGCAATTAAGGTG
Angptl	CTCGTCAGACATTCATCATCCAG	CACCTTCTTTTAGTGCAAAGGCT
Thpo	GGCCATGCTTCTTGCAGTG	AGTCGGCTGTGAAGGAGGT

Gapdh, glyceraldehyde 3-phosphate dehydrogenase; *cdh2*, N-cadherin; *Vcam-1*, vascular cell adhesion molecule-1; *Angptl*, angiopoietin-1; *Thpo*, thrombopoietin.

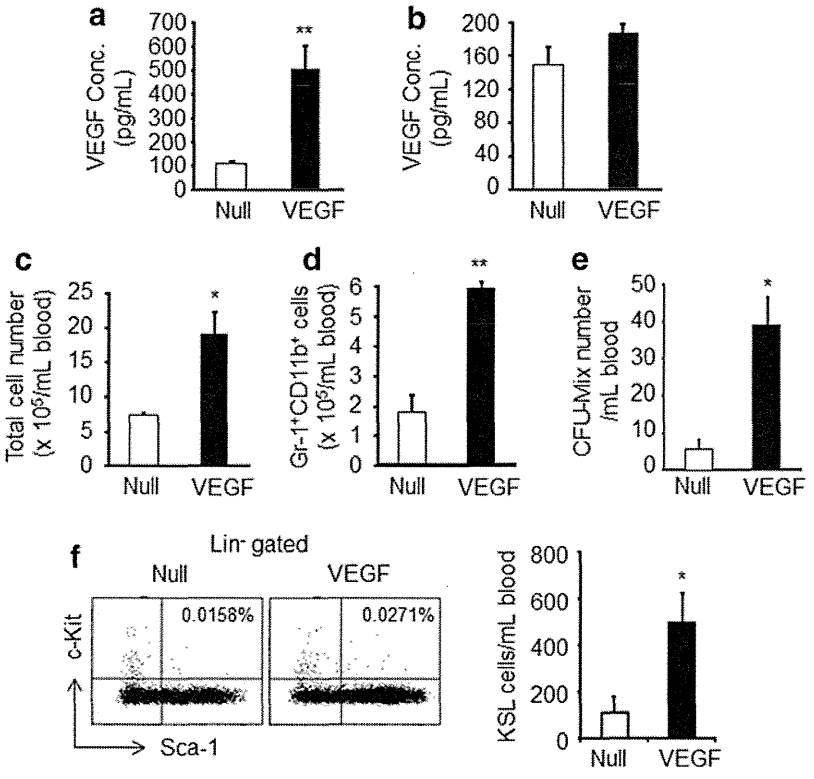

FIG. 1. Effect of vascular endothelial growth factor (VEGF) on the number of myeloid cells and hematopoietic stem/progenitor cells (HSPCs) in peripheral blood. **(a, b)** Mice were intravenously injected with adenovirus (Ad)-Null (Null) or Ad-VEGF (VEGF). Five days later, the concentration of plasma **(a)** and bone marrow (BM) **(b)** VEGF levels was determined by enzyme linked immunosorbent assay (ELISA). Data are expressed as mean ± standard deviation (SD) ($n=4$). **(c)** The number of total peripheral blood mononuclear cells (PBMCs) was counted on day 5 after administration of each Ad vector. **(d)** The percentage of Gr-1$^+$CD11b$^+$ myeloid cells was determined by flow cytometric analysis, and the absolute number was then normalized to the total PBMC number. Data are expressed as mean ± SD ($n=4$). **(e)** The number of colony forming unit (CFU)-Mix/CFU-granulocyte, erythroid, macrophage, megakaryocyte (GEMM) a multipotent hematopoietic progenitor cells, in PBMCs was determined by a standard colony assay. The colony number was normalized to the total PBMC number. **(f)** A representative analysis of the c-Kit$^+$Sca-1$^+$Lineage$^-$(KSL) subset in the blood is shown (*left*). The proportion of cKit$^+$Sca-1$^+$ cells in the lineage-negative (Lin$^-$) population is indicated in the dot blot. The number of KSL cells in the blood was normalized to the total cell number (*right*). Data are expressed as mean ± SD ($n=4$). *$P<0.05$, **$P<0.01$ as compared with Null.

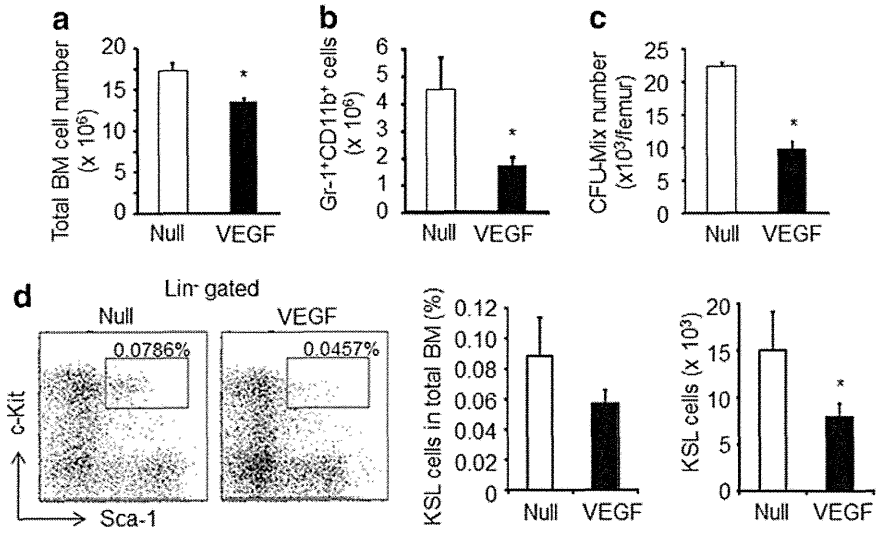

FIG. 2. Plasma elevation of VEGF leads to a decrease in the myeloid cells and HSPCs in the BM. **(a)** The number of total BM cells was counted on day 5 after Ad-Null or Ad-VEGF injection. **(b)** The number of Gr-1$^+$CD11b$^+$ cells in the BM was determined by flow cytometric analysis. **(c)** The number of CFU-Mix/CFU-GEMM in the BM was determined by a colony assay. The colony number was normalized to the total BM cell number. **(d)** A representative analysis of the KSL subset in the BM after administration of Ad-Null or Ad-VEGF is shown (*left*). The proportion of KSL cells in the total BM is indicated in the dot blot. Frequencies (*middle*) and absolute numbers (*right*) of KSL cells in the BM were calculated. Data are expressed as mean ± SD ($n=5$). *$P<0.05$ as compared with Null.

in the reduction in both the frequency and the absolute number of KSL cells in BM (Fig. 2d). Thus, these data suggest that VEGF exerts a physiological effect on the various types of cells within the BM.

Unchanged level of CXCL12 after VEGF overexpression

To examine the mechanisms of BM cell mobilization by VEGF treatment, we analyzed the expression levels of genes associated with HSC maintenance in the BM [*N-cadherin* (*cdh2*), *vascular cell adhesion molecule-1* (*Vcam-1*), *angiopoietin-1* (*Angpt1*), and *thrombopoietin* (*Thpo*)]. The expression levels of these genes in BM nonhematopoietic cells were modestly downregulated after Ad-VEGF injection (Fig. 3a). We next measured the CXCL12 levels in Ad-VEGF-injected mice. Chemokine CXCL12 is an indispensable factor for the maintenance and retention of HSPCs in the BM [5,24]. Previous studies showed that the BM CXCL12 levels were reduced by the injection of mobilization-inducing factors, such as G-CSF and stem cell factor (SCF) [10,25]. We also found that the CXCL12 levels were markedly reduced in the BM, but not the plasma, of Ad-G-CSF-injected mice (Fig. 3b). However, there was almost no difference in the BM CXCL12 levels between Ad-VEGF-injected mice and Ad-Null-injected mice (Fig. 3b). Therefore, these data indicate that VEGF would alter the BM microenvironment, probably by a different mechanism from other mobilization factors.

Reduction of MPCs in the BM after Ad-VEGF injection

Recent studies have demonstrated that MPCs play a pivotal role in HSPC maintenance in the BM [4,6–8]. Therefore, we examined the disposition of MPCs in the BM after Ad-VEGF administration. Flow cytometric analysis of the enzymatically dissociated BM cells revealed that Ad-VEGF overexpression led to a significant reduction of $CD45^-Ter119^-CD31^-Alcam^-Sca\text{-}1^+$ cells, which are reported to be MPCs [21,26] (Fig. 4a). In addition, the percentage of other MPC populations, such as $CD45^-Ter119^-PDGFR\alpha^+Sca\text{-}1^+$ cells [27] and $CD45^-Lineage^-CD31^-CD51^+Sca\text{-}1^+$ cells [28], in the BM of Ad-VEGF-injected mice was also lower than those of Ad-Null-injected mice (Fig. 4b, c). These data clearly showed the decreased number of phenotypically identified MPCs in the BM after injection of Ad-VEGF.

Next, to investigate whether functional MPCs in the BM were reduced in Ad-VEGF-injected mice, we performed a CFU-F assay and homing assay. Consistent with the above data, we observed decreased CFU-F numbers in the BM in Ad-VEGF-injected mice (Fig. 4d). For homing studies, Ad-Null- or Ad-VEGF-injected mice were used as the recipient mice. Donor BM cells derived from GFP transgenic mice were intravenously injected into nonirradiated recipient mice, and the frequency of GFP-expressing cells in the recipient BM was then estimated by flow cytometry. The results showed that the homing activity of GFP-expressing cells was partially inhibited in Ad-VEGF-treated recipient mice (Fig. 4e). Thus, the decreased homing efficiency of donor HSPCs in Ad-VEGF-injected mice suggests the decreased number of niche cells in the BM. Taken together, our findings indicate that overexpression of VEGF in mice leads to a reduction of phenotypic and functional MPCs in the BM.

VEGF stimulates the migration of MPCs

We next examined the mechanisms of the reduction of MPCs in the BM after VEGF overexpression. In vitro-expanded primary mouse BM stromal cells (mBMSCs), including MPCs, showed slight expression of Flt-1 (VEGFR1), but not Flk-1 (VEGFR2), on the cellular surface (Fig. 5a). We speculated that MPCs might egress from the BM in response to the plasma level of VEGF, because there was almost no change in the BM VEGF levels in Ad-VEGF-injected mice (Fig. 1b). We performed an in vitro migration assay and found a dose-dependent chemoattractive effect of VEGF on mBMSCs (Fig. 5b), suggesting the possibility that a decreased number of BM MPCs in Ad-VEGF-injected mice would result from the mobilization of MPCs to the peripheral tissue in response to an elevation of plasma VEGF.

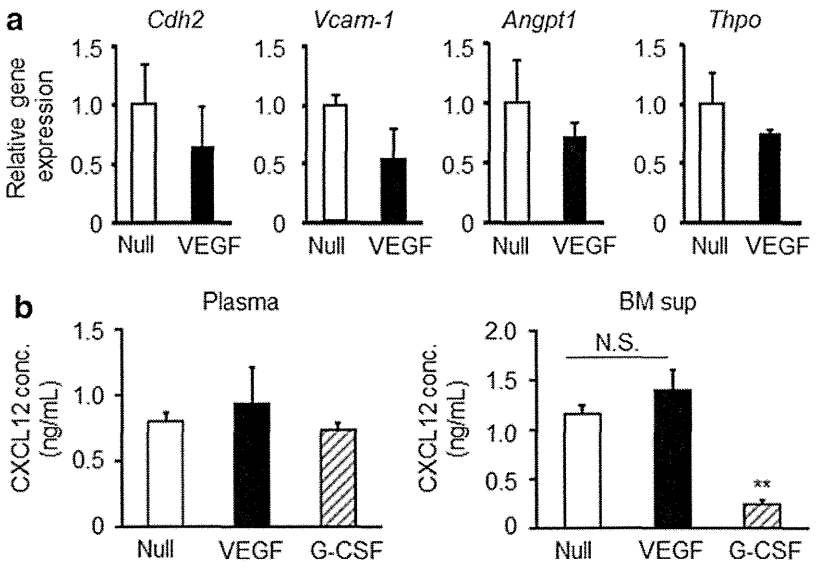

FIG. 3. Expression of HSPC maintenance factor genes after Ad-VEGF administration. **(a)** Expression levels of cadherin2 (Cdh2), vascular cell adhesion molecule-1 (Vcam-1), angiopoietin-1 (Angpt1), and thrombopoietin (Thpo) in nonhematopoietic cells ($CD45^-Ter119^-$ cells) were measured by quantitative polymerase chain reaction analysis. Data are expressed as mean ± SD ($n = 3$). **(b)** The plasma and BM supernatants of mice injected with Ad-Null, Ad-VEGF, or Ad-GCSF were collected. The levels of CXC chemokine ligand 12 (CXCL12) in the plasma (*left*) and the BM supernatant (*right*) were measured by ELISA. $^{**}P < 0.01$ as compared with Null. N.S. stands for not significant.

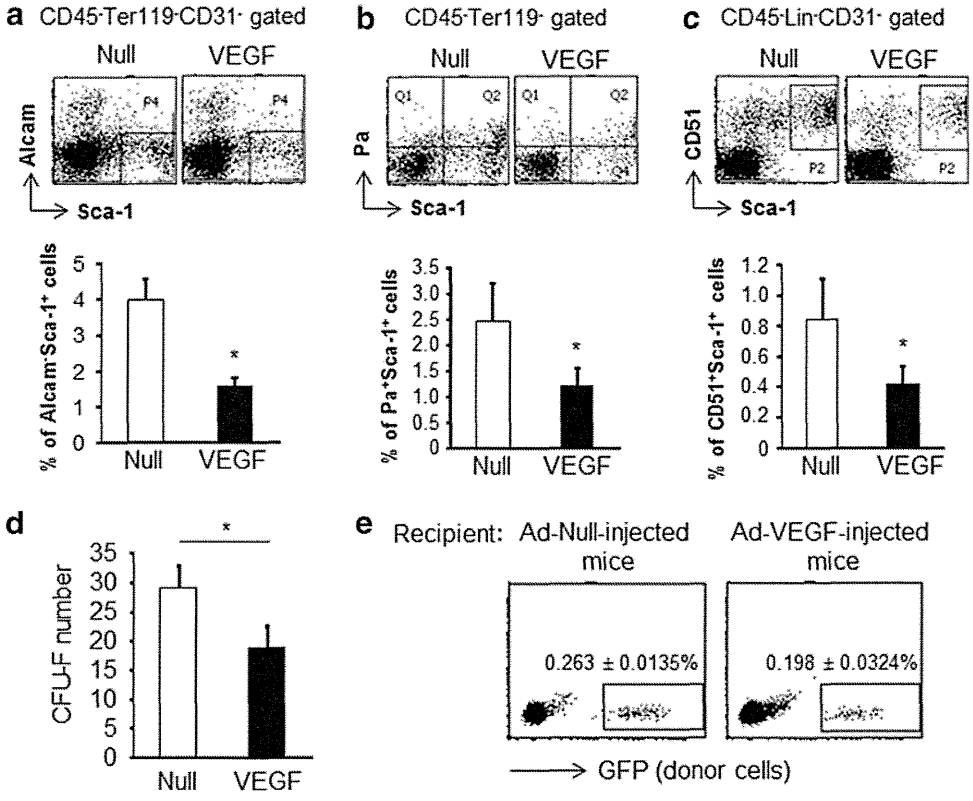

FIG. 4. The number of mesenchymal progenitor cells (MPCs) in the BM is decreased following Ad-VEGF injection. (**a–c**) After BM stromal cells were collected from bone by treatment with collagenase, the proportion of MPC populations [$CD45^-Ter119^-CD31^-Alcam^-Sca\text{-}1^+$ MPCs (**a**), $CD45^-Ter119^-$ $PDGFRa^+$ (Pa^+) $Sca\text{-}1^+$ MPCs (**b**), or Lin^-CD45^- $CD31^-CD51^+Sca\text{-}1^+$ MPCs (**c**)] in the BM was determined by flow cytometry. Data are expressed as mean ± SD ($n=5$). (**d**) A colony-forming unit-fibroblast (CFU-F) assay was performed using $CD45^-Ter119^-$ BM cells. The number of CFU-Fs was counted using a microscope after staining with the Giemsa solution. Data are expressed as mean ± SD ($n=3$). (**e**) Homing assay. After injection of Ad-Null or Ad-VEGF into mice, green fluorescent protein (GFP) transgenic mice-derived BM cells (donor cells) were transplanted into Ad vector-administrated mice. The percentage of donor cells (GFP-expressing cells) in the BM of Ad-Null- or Ad-VEGF-injected mice was analyzed by flow cytometry at 16 h after BM transplantation. The percentage of donor cells in the BM is indicated in the dot blot. Data are expressed as mean ± SD ($n=5$). *$P<0.05$ as compared with Null.

Discussion

Recent studies have clearly reported that the HSPC numbers in the BM are significantly decreased by conditional deletion of MPCs, including nestin-expressing stromal cells [4] and CXCL12-abundant reticular cells [5]. It is of note that deletion of MPCs led to the increased number of HSPCs in the spleen, demonstrating the mobilization of HSPCs from BM to peripheral tissues [4]. Therefore, maintenance and retention of HSPCs in the BM would

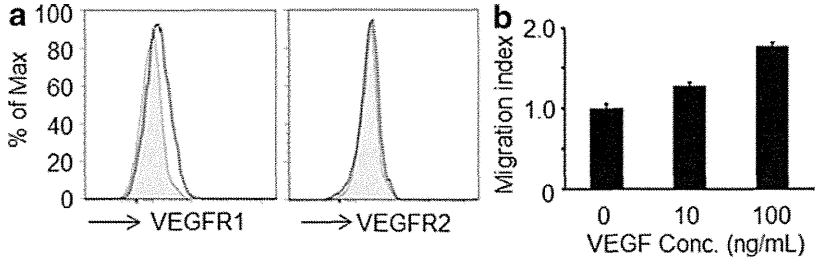

FIG. 5. VEGF enhances the migration capacity of MPCs. BM-derived stromal cells were collected and propagated in a tissue culture dish. (**a**) Expression levels of VEGF receptors, VEGFR1 (*left*) and VEGFR2 (*right*), in the cells was determined by flow cytometry. Staining profiles of specific mAb (*dotted lines*) and an isotype-matched control mAb (*gray area*) are shown. (**b**) BM stromal cells were exposed to various doses of recombinant VEGF. Cells that had migrated toward the VEGF (*lower chamber*) by passing through a membrane filter were counted by microscopy after staining with the Giemsa solution. Data are expressed as mean ± SD ($n=3$).

considerably be dependent on the number of MPCs [4,5]. In the present study, we examined the effect of VEGF on the disposition of BM HSPCs and MPCs in mice. Our main finding was that VEGF overexpression in mice resulted in a reduction of not only HSPCs but also MPCs in the BM. We also found that VEGF could promote the migration of mBMSCs in vitro. The data described here suggest that, as in the case of HSPCs, MPCs would also be mobilized to the peripheral tissues in response to an elevation of plasma VEGF levels, and a reduced number of BM MPCs by VEGF would lead to HSPC egress from the BM, because MPCs would function as niche cells in the BM.

It is well known that BM CXCL12 levels are down-regulated following G-CSF administration and thereby induce an egress of HSPCs [25,29]. Christopher et al. previously showed the reduced BM CXCL12 levels after administration of other mobilization factors, such as SCF and Flt3-ligand [10]. In addition to their mobilization-inducing effects, these factors also impact the number of stem and progenitor cells in the BM. For instance, it has been reported that the number of HSPCs and MPCs in the BM was significantly increased after G-CSF administration [30,31]. Unlike in the case of G-CSF and other mobilization factors, however, VEGF had almost no effect on BM CXCL12 levels (Fig. 3b). Furthermore, systemic VEGF expression resulted in a significant reduction in the number of HSPCs (KSL cells and CFU-Mix) in the BM (Fig. 2). The number of MPCs in the BM was also reduced in Ad-VEGF-injected mice (Fig. 4). Therefore, these data strongly indicate that VEGF would induce HSPC mobilization by altering the BM environment through different mechanisms from G-CSF. Notably, a recent study showed that HSPCs could be mobilized from the BM into the circulation by administration of a prostagrandin E_2 (PGE_2) inhibitor, and this effect was independent of CXCL12-CXCR4 signaling [32]. A nucleotide sugar, uridine diphosphate (UDP)-glucose, has also been shown to mobilize subsets of HSPCs functionally distinct from those mobilized by G-CSF, suggesting that UDP-glucose-induced HSPC mobilization would be mediated, at least in part, by different mechanisms from G-CSF [33]. Thus, it would be of interest to examine whether VEGF could influence the levels of BM PGE_2 and/or plasma UDP glucose.

The expression levels of HSC maintenance genes (*Cdh2*, *Vcam-1*, *Angpt1*, and *Thpo*) in BM nonhematopoietic cells were decreased in Ad-VEGF-injected mice (Fig. 3a). This would be due to the reduction in the number of MPCs in the BM after Ad-VEGF injection (Fig. 4). However, we have no idea why BM CXCL12 levels were not changed in Ad-VEGF-injected mice, because MPCs abundantly produce CXCL12 [7,8]. A detailed investigation would be required to clarify the regulation of CXCL12 expression in niche cells, including MPCs, endosteal osteoblasts, and endothelial cells.

We observed enhanced in vitro migration activities of mBMSCs by VEGF, suggesting the possibility that MPCs in the BM would be mobilized to the peripheral tissue in response to the plasma VEGF concentration. However, at present, we did not detect the CFU-F in the blood in Ad-VEGF-injected mice (data not shown). MPCs are known to be rare cells even in the BM, representing ~1 in 10,000–100,000 total nucleated cells [34], and it is therefore possible that the frequency of MPCs in the blood was too low to detect under our experimental conditions. Alternatively, it is also possible that VEGF overexpression in mice might lead to the homing of MPCs to organs, such as the liver, because transgene expression in the liver was extremely high following systemic Ad vector injection [35]. Therefore, it might be necessary to investigate whether or not the frequency and the number of MPCs are changed in tissues or organs other than the peripheral blood.

Recently, Liu et al. showed that MPCs could be mobilized to the peripheral tissue when rats were exposed to hypoxic conditions, and this hypoxia-induced MPC mobilization was caused by the elevation of plasma CXCL12 levels and BM VEGF levels [36]. Under our conditions, however, plasma CXCL12 levels and the BM VEGF levels in Ad-VEGF-injected mice were almost equal to those in Ad-Null-injected mice (Figs. 1b and 3b), suggesting that the mechanisms of decreased number of BM MPCs in Ad-VEGF-injected mice would be different from those of hypoxia-induced MPC mobilization.

Consistent with previous reports [15], we confirmed the HSPC mobilization from BM into the circulation by VEGF overexpression using an Ad vector system (Fig. 1). On the other hand, a previous report showed that administration of a recombinant VEGF protein into mice failed to induce the HSPC mobilization [37]. In our Ad vector systems, plasma VEGF levels were maintained at 400–600 ng/mL on day 3–5 after single intravenous injection. Although we do not know the VEGF levels in the plasma under their experimental protocols, plasma VEGF levels might not be sufficient for HSPC egress from the BM, because exogenous VEGF levels in the plasma were rapidly decreased after administration of a recombinant VEGF protein [23]. Therefore, this difference would be partly due to the difference in the plasma VEGF levels, and we concluded that an Ad vector system would be an appropriate one to estimate the in vivo physiological action of VEGF.

In summary, our results showed that plasma VEGF levels could regulate the distribution of BM HSPCs and MPCs, probably by a mechanism distinct from that of other mobilization factors, and we suggest that a reduction in the number of MPCs in the BM would be one of the mechanisms involved in VEGF-induced HSPC mobilization. Although further investigation of the BM environment will be needed to uncover the VEGF-mediated HSPC mobilization, our findings obtained in this study provide a novel insight into the mechanisms of HSPC mobilization and would be helpful in the development of new clinical mobilizing agents.

Acknowledgments

This work was supported by grants from the Ministry of Health, Labour, and Welfare of Japan, and by the Sasakawa Scientific Research Grant from the Japan Science Society.

Author Disclosure Statement

The authors have no financial conflict of interests.

References

1. Calvi LM, GB Adams, KW Weibrecht, JM Weber, DP Olson, MC Knight, RP Martin, E Schipani, P Divieti, et al.

(2003). Osteoblastic cells regulate the haematopoietic stem cell niche. Nature 425:841–846.
2. Zhang J, C Niu, L Ye, H Huang, X He, WG Tong, J Ross, J Haug, T Johnson, et al. (2003). Identification of the haematopoietic stem cell niche and control of the niche size. Nature 425:836–841.
3. Arai F, A Hirao, M Ohmura, H Sato, S Matsuoka, K Takubo, K Ito, GY Koh and T Suda. (2004). Tie2/angiopoietin-1 signaling regulates hematopoietic stem cell quiescence in the bone marrow niche. Cell 118:149–161.
4. Mendez-Ferrer S, TV Michurina, F Ferraro, AR Mazloom, BD Macarthur, SA Lira, DT Scadden, A Ma'ayan, GN Enikolopov and PS Frenette. (2010). Mesenchymal and haematopoietic stem cells form a unique bone marrow niche. Nature 466:829–834.
5. Omatsu Y, T Sugiyama, H Kohara, G Kondoh, N Fujii, K Kohno and T Nagasawa. (2010). The essential functions of adipo-osteogenic progenitors as the hematopoietic stem and progenitor cell niche. Immunity 33:387–399.
6. Ding L, TL Saunders, G Enikolopov and SJ Morrison. (2012). Endothelial and perivascular cells maintain haematopoietic stem cells. Nature 481:457–462.
7. Ding L and SJ Morrison. (2013). Haematopoietic stem cells and early lymphoid progenitors occupy distinct bone marrow niches. Nature 495:231–235.
8. Greenbaum A, YM Hsu, RB Day, LG Schuettpelz, MJ Christopher, JN Borgerding, T Nagasawa and DC Link. (2013). CXCL12 in early mesenchymal progenitors is required for haematopoietic stem-cell maintenance. Nature 495:227–230.
9. Mendez-Ferrer S, D Lucas, M Battista and PS Frenette. (2008). Haematopoietic stem cell release is regulated by circadian oscillations. Nature 452:442–447.
10. Christopher MJ, F Liu, MJ Hilton, F Long and DC Link. (2009). Suppression of CXCL12 production by bone marrow osteoblasts is a common and critical pathway for cytokine-induced mobilization. Blood 114:1331–1339.
11. Carmeliet P, V Ferreira, G Breier, S Pollefeyt, L Kieckens, M Gertsenstein, M Fahrig, A Vandenhoeck, K Harpal, et al. (1996). Abnormal blood vessel development and lethality in embryos lacking a single VEGF allele. Nature 380:435–439.
12. Ferrara N, K Carver-Moore, H Chen, M Dowd, L Lu, KS O'Shea, L Powell-Braxton, KJ Hillan and MW Moore. (1996). Heterozygous embryonic lethality induced by targeted inactivation of the VEGF gene. Nature 380:439–442.
13. Gerber HP, AK Malik, GP Solar, D Sherman, XH Liang, G Meng, K Hong, JC Marsters and N Ferrara. (2002). VEGF regulates haematopoietic stem cell survival by an internal autocrine loop mechanism. Nature 417:954–958.
14. Chan CK, CC Chen, CA Luppen, JB Kim, AT DeBoer, K Wei, JA Helms, CJ Kuo, DL Kraft and IL Weissman. (2009). Endochondral ossification is required for haematopoietic stem-cell niche formation. Nature 457:490–494.
15. Hattori K, S Dias, B Heissig, NR Hackett, D Lyden, M Tateno, DJ Hicklin, Z Zhu, L Witte, et al. (2001). Vascular endothelial growth factor and angiopoietin-1 stimulate postnatal hematopoiesis by recruitment of vasculogenic and hematopoietic stem cells. J Exp Med 193:1005–1014.
16. Mizuguchi H and MA Kay. (1998). Efficient construction of a recombinant adenovirus vector by an improved *in vitro* ligation method. Hum Gene Ther 9:2577–2583.
17. Mizuguchi H and MA Kay. (1999). A simple method for constructing E1- and E1/E4-deleted recombinant adenoviral vectors. Hum Gene Ther 10:2013–2017.
18. Xu ZL, H Mizuguchi, A Ishii-Watabe, E Uchida, T Mayumi and T Hayakawa. (2001). Optimization of transcriptional regulatory elements for constructing plasmid vectors. Gene 272:149–156.
19. Sakurai H, K Tashiro, K Kawabata, T Yamaguchi, F Sakurai, S Nakagawa, H Mizuguchi. (2008). Adenoviral expression of suppressor of cytokine signaling-1 reduces adenovirus vector-induced innate immune responses. J Immunol 180: 4931–4938.
20. Koizumi N, H Mizuguchi, N Utoguchi, Y Watanabe and T Hayakawa. (2003). Generation of fiber-modified adenovirus vectors containing heterologous peptides in both the HI loop and C terminus of the fiber knob. J Gene Med 5:267–276.
21. Nakamura Y, F Arai, H Iwasaki, K Hosokawa, I Kobayashi, Y Gomei, Y Matsumoto, H Yoshihara and T Suda. (2010). Isolation and characterization of endosteal niche cell populations that regulate hematopoietic stem cells. Blood 116:1422–1432.
22. Okabe M, M Ikawa, K Kominami, T Nakanishi and Y Nishimune. (1997). 'Green mice' as a source of ubiquitous green cells. FEBS Lett 407:313–319.
23. Gabrilovich D, T Ishida, T Oyama, S Ran, V Kravtsov, S Nadaf and DP Carbone. (1998). Vascular endothelial growth factor inhibits the development of dendritic cells and dramatically affects the differentiation of multiple hematopoietic lineages *in vivo*. Blood 92:4150–4166.
24. Sugiyama T, H Kohara, M Noda and T Nagasawa. (2006). Maintenance of the hematopoietic stem cell pool by CXCL12-CXCR4 chemokine signaling in bone marrow stromal cell niches. Immunity 25:977–988.
25. Petit I, M Szyper-Kravitz, A Nagler, M Lahav, A Peled, L Habler, T Ponomaryov, RS Taichman, F Arenzana-Seisdedos, et al. (2002). G-CSF induces stem cell mobilization by decreasing bone marrow SDF-1 and up-regulating CXCR4. Nat Immunol 3:687–694.
26. Ikushima YM, F Arai, K Hosokawa, H Toyama, K Takubo, T Furuyashiki, S Narumiya and T Suda. (2013). Prostaglandin E(2) regulates murine hematopoietic stem/progenitor cells directly via EP4 receptor and indirectly through mesenchymal progenitor cells. Blood 121:1995–2007.
27. Morikawa S, Y Mabuchi, Y Kubota, Y Nagai, K Niibe, E Hiratsu, S Suzuki, C Miyauchi-Hara, N Nagoshi, et al. (2009). Prospective identification, isolation, and systemic transplantation of multipotent mesenchymal stem cells in murine bone marrow. J Exp Med 206:2483–2496.
28. Winkler IG, NA Sims, AR Pettit, V Barbier, B Nowlan, F Helwani, IJ Poulton, N van Rooijen, KA Alexander, LJ Raggatt and JP Levesque. (2010). Bone marrow macrophages maintain hematopoietic stem cell (HSC) niches and their depletion mobilizes HSCs. Blood 116:4815–4828.
29. Levesque JP, J Hendy, Y Takamatsu, PJ Simmons and LJ Bendall. (2003). Disruption of the CXCR4/CXCL12 chemotactic interaction during hematopoietic stem cell mobilization induced by GCSF or cyclophosphamide. J Clin Invest 111:187–196.
30. Brouard N, R Driessen, B Short and PJ Simmons. (2010). G-CSF increases mesenchymal precursor cell numbers in the bone marrow via an indirect mechanism involving osteoclast-mediated bone resorption. Stem Cell Res 5:65–75.
31. Grassinger J, B Williams, GH Olsen, DN Haylock and SK Nilsson. (2012). Granulocyte colony stimulating factor

expands hematopoietic stem cells within the central but not endosteal bone marrow region. Cytokine 58:218–225.
32. Hoggatt J, KS Mohammad, P Singh, AF Hoggatt, BR Chitteti, JM Speth, P Hu, BA Poteat, KN Stilger, et al. (2013). Differential stem- and progenitor-cell trafficking by prostaglandin E2. Nature 495:365–369.
33. Kook S, J Cho, SB Lee and BC Lee. (2013). The nucleotide sugar UDP-glucose mobilizes long-term repopulating primitive hematopoietic cells. J Clin Invest 123:3420–3435.
34. Chamberlain G, J Fox, B Ashton and J Middleton. (2007). Concise review: mesenchymal stem cells: their phenotype, differentiation capacity, immunological features, and potential for homing. Stem Cells 25:2739–2749.
35. Koizumi N, T Yamaguchi, K Kawabata, F Sakurai, T Sasaki, Y Watanabe, T Hayakawa and H Mizuguchi. (2007). Fiber-modified adenovirus vectors decrease liver toxicity through reduced IL-6 production. J Immunol 178:1767–1773.
36. Liu L, Q Yu, J Lin, X Lai, W Cao, K Du, Y Wang, K Wu, Y Hu, et al. (2011). Hypoxia-inducible factor-1alpha is essential for hypoxia-induced mesenchymal stem cell mobilization into the peripheral blood. Stem Cells Dev 20:1961–1971.
37. Pitchford SC, RC Furze, CP Jones, AM Wengner and SM Rankin. (2009). Differential mobilization of subsets of progenitor cells from the bone marrow. Cell Stem Cell 4:62–72.

Address correspondence to:
Dr. Kenji Kawabata
Laboratory of Stem Cell Regulation
National Institute of Biomedical Innovation
7-6-8, Saito-Asagi
Ibaraki, Osaka 567-0085
Japan

E-mail: kawabata@nibio.go.jp

Received for publication September 27, 2013
Accepted after revision December 16, 2013
Prepublished on Liebert Instant Online December 17, 2013

Neuroscience Letters 590 (2015) 126–131

Contents lists available at ScienceDirect

Neuroscience Letters

journal homepage: www.elsevier.com/locate/neulet

Research article

An inhibitory pathway controlling the gating mechanism of the mouse lateral amygdala revealed by voltage-sensitive dye imaging

Tomomi Fujieda[a,b], Noriko Koganezawa[b], Yoshinori Ide[a], Tomoaki Shirao[b], Yuko Sekino[a,b,*]

[a] Division of Pharmacology, National Institute of Health Sciences, 1-18-1 Kamiyoga, Setagaya-ku, Tokyo 158-8501, Japan
[b] Department of Neurobiology and Behavior, Gunma University Graduate School of Medicine, 3-39-22 Showa-machi, Maebashi, Gunma 371-8511, Japan

HIGHLIGHTS

- EC stimulation induces large and long-lasting hyperpolarizing signals in the La.
- This hyperpolarization is analyzed by VSD imaging spatially and temporally.
- We identify an inhibitory pathway toward the La via the m-ITC.

ARTICLE INFO

Article history:
Received 14 January 2015
Received in revised form 28 January 2015
Accepted 29 January 2015
Available online 31 January 2015

Keywords:
External capsule
GABAergic neurons
Hyperpolarization
Lateral amygdala
Medial intercalated cluster
Voltage-sensitive dye imaging

ABSTRACT

The lateral amygdala nucleus (La) is known as a gateway for emotional learning that interfaces sensory inputs from the cortex and the thalamus. In the La, inhibitory GABAergic inputs control the strength of sensory inputs and interfere with the initial step of the acquisition of fear memory. In the present study, we investigated the spatial and temporal patterns of the inhibitory responses in mouse La using voltage-sensitive dye imaging. Stimulating the external capsule (EC) induced large and long-lasting hyperpolarizing signals in the La. We focused on these hyperpolarizing signals, revealing the origins of the inhibitory inputs by means of surgical cuts on the possible afferent pathways with four patterns. Isolating the medial branch of EC (ECmed), but not the lateral branch of EC (EClat), from the La strongly suppressed the induction of the hyperpolarization. Interestingly, isolating the ECmed from the caudate putamen did not suppress the hyperpolarization, while the surgical cut of the ECmed fiber tract moderately suppressed it. Glutamatergic antagonists completely suppressed the hyperpolarizing signals induced by the stimulation of EC. When directly stimulating the dorsal, middle or ventral part of the ECmed fiber tract in the presence of glutamatergic antagonists, only the stimulation in the middle part of the ECmed caused hyperpolarization. These data indicate that the GABAergic neurons in the medial intercalated cluster (m-ITC), which receive glutamatergic excitatory input from the ECmed fiber tract, send inhibitory afferents to the La. This pathway might have inhibitory effects on the acquisition of fear memory.

1. Introduction

The amygdala is an important brain structure for emotional behavior and learning [13]. Fear conditioning is a widely-used experimental model to examine emotional and learning processing in animal brains. The lateral amygdala nucleus (La) is known as a gateway for emotional learning that interfaces sensory inputs from the cortex and the thalamus [14]. Inhibitory circuits are known to control the amygdala's functions, such as acquisition, expression, and extinction of conditioned fear [6,21,22]. Inhibitory inputs to the La control the strength of sensory inputs and interfere with the initial step of the acquisition of fear memory. Two groups of GABAergic neurons in the amygdala are known: local interneurons that are scattered within the local neuropil [17], and intercalated cells organized in clusters (intercalated clusters) surrounding the amygdala complex [15,16,18,20,23,24]. Although inhibitory inputs to the individual principal neurons in the amygdala have been analyzed electrophysiologically [4,26,31,37,38], how sensory inputs

* Corresponding author at: Division of Pharmacology, National Institute of Health Sciences, 1-18-1 Kamiyoga, Setagaya-ku, Tokyo 158-8501, Japan.
Tel.: +81 3 3700 9692; fax: +81 3 3700 1452.
E-mail address: yukos@nihs.go.jp (Y. Sekino).

http://dx.doi.org/10.1016/j.neulet.2015.01.079

induce inhibitory responses in the La, and how inhibitory responses propagate in the La, are still unclear because of the technical limitations of patch clamp recording.

Optical imaging techniques overcome these limitations to investigating propagations in a wide range of neuronal interactions, and have been applied in the study of excitatory circuits of several brain regions [7,9,11,12,29,33,34]. In this study, using optical imaging techniques, we investigate neuronal activities in the La, focusing particularly on inhibitory responses. To identify the origins of the inhibitory inputs, we perform various patterns of knife-cut operations of the possible afferent pathways evoking hyperpolarization in the La. In addition, we investigate the effects of glutamatergic antagonists on the inhibitory responses in the La, and show an inhibitory pathway from the medial intercalated cluster (m-ITC) to the La.

2. Materials and methods

2.1. Slice preparation and staining procedure

The experimental protocol was reviewed and approved by the National Institute of Health Sciences (NIHS) in Japan, following the guidelines in the National Research Council's 'Guide for the Care and Use of Laboratory Animals'. All experiments were approved by the NIHS' ethics committee. Male mice (C57BL/6 J, 7–22 weeks old, Japan SLC, Inc., Japan) were deeply anesthetized with halothane and quickly decapitated. Coronal slices containing the amygdala complex (400 μm) were prepared using a vibrating microtome (Campden Instruments Ltd., Loughborough, UK) in ice-cold artificial cerebrospinal fluid (ACSF). The ACSF was composed of the following (in mM): 119 NaCl, 2.5 KCl, 1.3 $MgSO_4$, 2.5 $CaCl_2$, 1.0 NaH_2PO_4, 26.2 $NaHCO_3$, and 11.0 glucose; this was oxygenated with a mixture gas of 95% O_2 and 5% CO_2 (pH 7.4). The slices were immediately soaked in the oxygenated ACSF containing a voltage-sensitive dye (VSD), di-4-ANEPPS (50 μM, Invitrogen Molecular Probes Inc., Oregon, USA) for 10 s, and then transferred to a filter that absorbed the staining solution and subsequently to another filter that absorbed the normal ACSF for at least an hour before the experiment.

2.2. Experimental apparatus for VSD imaging

An epi-illumination macro zoom fluorescence microscopy (MVX-10 MacroView, Olympus, Japan), a LED light source with a 530 nm center wavelength (LEX2-Green, Brainvision Inc., Tokyo, Japan), a dichroic mirror (560 nm), an emission filter (BP 575–625 nm), and a CMOS imaging device (MiCAM ULTIMA-L, Brainvision Inc., Tokyo) were used for VSD imaging.

The decrease and increase in the fluorescent intensity from the preparation corresponded to the membrane depolarization and hyperpolarization, respectively. Each data acquisition consisted of 1024 images of consecutive frames (1.0 ms/frame). A coaxial needle electrode (TF203-047, Unique Medical Co. Ltd., Tokyo, Japan) was placed on the external capsule (EC). Electrical stimuli with 200-μs duration at various intensities from 15 to 90 μA were delivered at the 100th frame of each acquisition. To analyze the effects of deafferentation on the induction of the hyperpolarization, the stimulus intensity was adjusted to make the peak value of depolarization equal before and after the surgical cut. Methods to calculate optical signals and present images were described in previous papers [11,29,32].

2.3. Surgical cuts of afferent connections to the La

After recording the optical signals at various stimulation intensities, we performed knife-cut operations on the pathways assumed to be involved in the induction of the hyperpolarization in the La. Four afferent pathways to the La were cut under the macro scope observation, as follows: the La was isolated by the longitudinal cut from: (i) the lateral branch of the EC, (ii) the medial branch of the EC and (iii) the CPu, and by (iv) the transverse cut of ECmed at the dorsal part. For the sham operations, the slices remained intact but the same procedure was carried out. After the surgical cuts, the slices were stored in the recovery chamber at room temperature (at least 1 h).

2.4. Excitation and inhibition values

Images from the 251st–300th frames were stacked and averaged to determine regions of interest (ROIs), which were circles of 8 pixels in diameter. Two ROIs were defined for each experiment. One of the ROIs had the maximal hyperpolarization value in the center spot. The other was adjacent to the first, which had an adequately large hyperpolarization value within the region. For the after-operation analysis, the ROIs were centered on the spots that had the same distances from the position of the stimulating electrode and the EC as the before-operation analysis. The averaged optical signals of the two ROIs were used as representative data.

The excitation (E) value was determined as the largest value among all the values from the first to the 15th frame after electrical stimulation. The inhibition (I) value was determined by averaging 50 frames, from the 251st frame to the 300th frame after the electrical stimulation.

2.5. Statistical analysis

We defined the operation index (OI) as follows: $OI = [I/E]_a/[I/E]_b$, where a: after the operation, b: before the operation. The data were presented as mean ± standard error of the mean (SEM). Normality of the data was tested with the Shapiro–Wilk test, and subsequently one-way ANOVA followed by Dunnett's post-hoc test was carried out. In the pharmacological experiments, inhibition value was statistically analyzed using a paired t-test.

3. Results

3.1. Optical signal propagation after the EC stimulation

The anatomical nomenclatures related to our experiments are shown in Fig. 1A. Each white fiber bundle in the amygdala slice preparation was observed through the macro zoom microscope; thus, the ramifying point of the EC was identified. The La, BLA, and CeA of the amygdala complex were identified in the fluorescent image recorded by the system (Fig. 1B). In Fig. 1C, a typical example of the optical signal propagation is shown in pseudo-color representation. The depolarization started at the stimulation point and spread over the La within 3 ms after the stimulation (0–3 ms). It became stronger in the La and spread over the other regions, the BLA, CPu, and CeA (4–7 ms). Then the depolarization at the dorsal area of the La faded, while growing stronger in the other regions (8–11 ms). Following depolarization, a weak hyperpolarization was first observed in the La; the depolarization remained in the other regions, although it was weakened (12–15 ms). The hyperpolarization grew stronger, and the depolarization in the other regions gradually disappeared (16–19 ms). The hyperpolarization in the La lasted about 600–650 ms (the middle wave in Fig. 1B). The maximal value of the hyperpolarization was observed around 255 ms after the stimulation.

After the hyperpolarization started in the La at the area along the dorsal part of the ECmed (16–19 ms), it spread out in the La during the next 100 ms (20–119 ms), then it spread over the BLA and a narrow part of the CPu along the dorsal part of the ECmed